# Progressive ductile shearing during till accretion within the deforming bed of a palaeo-ice stream

Emrys Phillips [1]*, Matteo Spagnolo [2], Alasdair C.J. Pilmer [2], Brice R. Rea [2], Jan A. Piotrowski [3], Jeremy C. Ely[4] and Simon Carr [5]

1 British Geological Survey, The Lyell Centre, Research Avenue South, Edinburgh EH14 4AP, UK

2 Department of Geography and the Environment, School of Geosciences, University of Aberdeen, Aberdeen AB24 3UF, UK

3 Department of Geoscience, Aarhus University, Denmark

4 Department of Geography, University of Sheffield, Sheffield S10 2TN, UK

5 School of Geography, Queen Mary, University of London, Mile End Road, London E1 4NS, UK

* Corresponding author: e-mail - erp@bgs.ac.uk

**Keywords:** micromorphology; glacier bed deformation; ductile shearing; foliation development; palaeo-ice stream

## Abstract

This paper presents the results of a detailed microstructural study of a thick till formed beneath the Weichselian (Devensian) Odra palaeo-ice stream, west of Środa Wielkopolska, Poland. This SE-flowing ice stream was one of a number of corridors of faster flowing ice which drained the Scandinavian Ice Sheet in the Baltic region. Macroscopically, the massive, laterally extensive till which formed the bed of this ice stream lacks any obvious evidence of glaciotectonism (thrusting, folding). However, microscale analysis reveals that bed deformation was dominated by foliation development, recording progressive ductile shearing within a subhorizontal subglacial shear zone. Five successive generations of clast microfabric (S1 to S5) have been identified defining a set of up-ice and down-ice dipping Riedel shears, as well as a subhorizontal shear foliation coplanar to the ice-bed interface. Cross-cutting relationships between the shear fabrics record temporal changes in the style of deformation during this progressive shear event. Kinematic indicators (S-C and ECC-type fabrics) within the till indicate a consistent SE-directed shear sense, in agreement with the regional ice flow pattern. A model of bed deformation involving incremental progressive simple shear during till accretion is proposed. The relative age of this deformation was diachronous becoming progressively younger upwards, compatible with subglacial shearing having accompanied till accretion at the top of the deforming bed. Variation in the relative intensity of the microfabrics

records changes in the magnitude of the cumulative strain imposed on the till and the degree of coupling between the ice and underlying bed during fast ice flow.

# 1. Introduction

Ice streams play an important role in regulating the behaviour of modern ice sheets (e.g. Antarctica, Bamber *et al*., 2000) and take the form of corridors of fast flowing ice bounded by ice flowing up to an order of magnitude slower (Stokes and Clark, 2001; Bennett, 2003). However the factors controlling fast ice flow are incompletely understood. Published studies of modern and ancient ice stream beds have led to two possible explanations governing ice stream flow: (i) basal sliding facilitated by elevated water pressures at the ice-bed interface with the ice stream effectively becoming decoupled from the underlying sediments (e.g. Alley, 1989; Piotrowski and Tulaczyk, 1999) or hard bedrock substrate (Margold *et al*., 2015); and (ii) basal motion accommodated by deformation of either a thick (several metres) or thin (centimetres to decimetres) layer of 'soft' sediments (till) (e.g. Alley *et al*., 1986, 1987a, b; Boulton and Hindmarsh, 1987; Clarke, 1987; Humphrey *et al*., 1993; Boulton *et al*., 2001). However, in reality these two processes are not mutually exclusive and may periodically "switch" to form the dominant movement mechanism of ice stream movement depending upon the water content and/or pressure within the bed. Understanding these processes has fundamental implications for our understanding of subglacial sediment erosion, transport and deposition. Furthermore a greater understanding of the subglacial environment of ice streams may also elucidate controls on ice streaming such as basal thermal regime (Hindmarsh, 2009) and/or subglacial hydrology (Kyrke-Smith *et al*., 2015), leading to the development of more sophisticated and robust models of ice stream flow dynamics and, ultimately, ice sheet mass balance and sea-level change.

The recognition of a characteristic suite of subglacial landforms (including megascale glacial lineations) formed beneath palaeo-ice streams (e.g. Dyke and Morris, 1988; Hodgson, 1994; Patterson, 1997, 1998; Clark and Stokes, 2001, 2002, 2003) has enabled the establishment of a set of criteria for identifying the presence and areal extent of these ancient ice streams (Stokes and Clark, 1999). These criteria have been, at least partially, validated by observations of the subglacial landscape beneath contemporary Antarctic ice-streams (King *et al*., 2009; Bingham *et al*., 2017). The exposed beds of palaeo-ice streams provide an ideal laboratory to investigate the sedimentary and structural processes occurring beneath fast flowing ice. However, on a macroscale the sediments (tills) deposited beneath many palaeo-ice streams are massive, lacking any visible signs of stratification and/or glacitectonic deformation (see Evans, 2018 and references therein). As a consequence micromorphology is increasingly being used as a primary tool for the analysis of these and other subglacial sediments (tills) (see Menzies and Maltman, 1992; van der Meer, 1979, 1987; Menzies *et al*., 1997; Khatwa and Tulaczyk, 2001; van der Meer *et al*., 2003; Hiemstra *et al*., 2005; Baroni and Fasano, 2006; Larsen *et al*., 2006, 2007; Phillips *et al*., 2007, 2011, 2013, 2018; Narloch *et al*., 2012; Neudorf *et al*., 2013; Gehrmann *et al*., 2017; Evans, 2018). This technique can provide far greater detail on the depositional and deformation histories recorded by these sediments than can be obtained from macroscale studies alone; for example, unravelling the often complex deformation histories recorded by glacigenic sequences (van der Meer, 1993; Phillips and Auton, 2000; van der Wateren *et al*., 2000; Menzies, 2000; Phillips *et al*., 2007; Lee and Phillips, 2008; Vaughan-Hirsch *et al*., 2013; Narloch *et al*., 2012, 2013) and the role played by pressurised meltwater during their deformation (Hiemstra and van der Meer, 1997; Phillips and Merritt, 2008; van der Meer *et al*., 2009; Denis *et al*., 2010; Phillips *et al*., 2013; 2018; Narloch *et al*., 2012, 2013).

This paper presents the results of a detailed micromorphological study of the thick till sequence laid down by the Weichselian (Devensian) Odra palaeo-ice stream as it flowed SE across Wielkopolska Lowlands of Poland (Fig. 1). The study area is located near Poznań, in a region dominated by NW-SE-trending subglacial landforms (megascale lineations) interpreted as having been formed during fast ice flow (Przybylski, 2008; Spagnolo *et al*., 2016). Thin sections are used to investigate the strain signature imparted by this palaeo-ice stream on the laterally extensive till formed within its bed. The results of this detailed microstructural study have been used to investigate the nature of deformation and in particular foliation development during progressive ductile simple shear within an evolving subhorizontal subglacial shear zone. Spatial variations in the relative intensity of the microfabrics are interpreted as recording changes in the magnitude of the cumulative strain imposed on the till, potentially reflecting the degree of ice-bed coupling during fast ice flow.

## 2. Location of study area and geological setting

During the Weichselian (Devensian) glaciation much of the Baltic region was covered by the Scandinavian Ice Sheet. This ice sheet was drained by a series of ice streams, including the Odra palaeo-ice stream (OPIS) which flowed SE across the Wielkopolska Lowland region of western Poland (Przybylski, 2008; Spagnolo *et al*., 2016). In this region, the bed of the Odra palaeo-ice stream (over 1000 km$^2$) is characterised by a suite of well-preserved NW-SE-trending megascale glacial lineations (MSGL) underlain by a thick (c. 30 m) sequence of Quaternary sediments. This study is focused on the bed of the OPIS to the west of the town of Środa Wielkopolska, approximately 30 km southeast of Poznań (Fig. 1a, b), close to the c. 21 ka Leszno phase ice margin (Kozarski, 1988; Przybylski, 2008; Marks, 2012). The geomorphology of the study area (c. 180 km$^2$) is dominated by a suite of elongate

(>16 km long), low-relief (2-4 m high) MSGL with a crest-to-crest spacing of 600-800 m (Fig. 1c). It is possible that these landforms were originally much longer (Przybylski, 2008) as they have been locally truncated by glacifluvial erosion, as well as the extensive urbanisation of the region which has locally overprinted/strongly modified this subglacial landscape. Although locally modified the morphology of these subglacial landforms are comparable to MSGL described from other palaeo-ice stream settings worldwide (Spagnolo *et al*., 2014).

The sediments making up the bed of the OPIS are in general poorly exposed and detailed sedimentological analysis of these deposits has relied upon trenches excavated at key positions across the MSGL's (Fig. 1c; see below). The trenches reveal that these subglacial landforms are composed of a homogeneous, matrix-supported, yellow coloured silty-sandy diamicton (Fig. 1d) containing rare gravel (2-64 mm) and extremely rare cobble (>64 mm) sized clasts (Spagnolo *et al*., 2016). The massive, laterally extensive diamicton (interpreted as a subglacial traction till; sensu Evans *et al*., 2006) lacks any obvious macroscale evidence of glaciotectonism (e.g. thrusting, folding… etc.) and no other sedimentary units have been recognised. Fine gravel clasts (2-4 mm) contained within the diamicton are composed of a range of sedimentary and crystalline rock fragments, including Palaeozoic limestones derived from the Baltic Basin as well as metamorphic and igneous rocks from Scandinavia, indicating that this deposit contains a significant far-travelled component (Spagnolo *et al*., 2016). The diamicton is relatively unaltered, exhibiting only very minor to rare macroscopic evidence of calcification, typically occurring in patches of <200 $cm^2$. Clast a-axis macrofabric data published by Spagnolo *et al*. (2016) are remarkably uniform (vertically and laterally) across the bed of the OPIS within the study area. These shallow dipping macrofabrics are orientated NW-SE, concordant with the long axes of the MSGL and parallel to the regional ice flow direction.

## 3. Methods

Detailed analysis of the till forming the bed of the OPIS has focussed on 10 sites located on the crests (A, B, C, D, E, K, T; Fig. 1c) and flanks (X, Y, Z; Fig. 1c) of three of the mega-scale lineations. A trench (6-10 m long, 2-3 m wide and 3-5 m deep) was excavated at each site (Fig. 1d) and the samples for thin section preparation collected using standard Kubiena tins. Prior to sampling, the temporarily exposed sections were logged, photographed and described in detail with particular emphasis being placed on recording the macroscale variation in lithology and structure of the till. The samples were collected in a vertical profile (e.g. C1M highest to C6M lowest) below the base of the modern soil and with a 20 cm spacing between each Kubiena tin (Fig. 1d). This approach was adopted to provide detailed information on the range of microstructures developed at different stratigraphical/structural levels within the till. The Kubiena tins were either cut or pushed into the face in order to limit sample disturbance. The position of the sample within the sequence, its orientation relative to magnetic north, depth and way-up were marked on the outside of the tin during collection.

Sample preparation was carried out at Royal Holloway, University of London, using the methods outlined by Palmer (2005). Large format (10 x 8 cm), orientated (parallel to the long axis of the MSGL and former ice flow direction) thin sections were taken from the centre of each of the resin impregnated samples, avoiding artefacts associated with sample collection. The thin sections were described using a Zeiss petrological microscope revealing that the composition, texture and structure of the diamicton are uniform across the study area. The detailed microscale study focused upon site C, located on the crest of a prominent NW-SE-trending MSGL, as well as three samples from sites X, Y and Z, which provide a traverse across the flank of one of these landforms (Fig. 1c). The location of site C on the crest of the MSGL means that the thin sections represent a vertical section through the landform and therefore provide a valuable insight into the processes which may have occurred during the formation of this landform. The terminology used to describe the various microtextures developed within these sediments follows that proposed by van der Meer (1987, 1993) and Menzies (2000) with modifications. Microstructural maps and quantitative data for the clast microfabrics (Figs. 2 to 7) developed within the till were obtained using the methodology of Phillips *et al*. (2011) (also see Vaughan-Hirsh *et al*., 2013; Neudorf *et al*., 2013; Gehrmann *et al*., 2017; Phillips *et al*., 2013, 2018; Brumme, 2015). During this process the relationships between successive generations of clast microfabrics (S1 oldest to Sn youngest) and other microstructures (e.g. plasmic fabrics, turbate structures, folds, faults, shears…etc) present within the diamicton are determined, allowing a detailed relative chronology of fabric development to be established, enabling the investigation of the complex polyphase deformation histories recorded in these deposits (see Phillips *et al*., 2011 for details of this process). Each thin section was divided into 16 rectangular areas (A to P on Figs. 2 to 7) and the orientation of the long axes of the clasts (skeleton grains) plotted on a series of rose diagrams and the eigenvalues (E1, E2) calculated for each area using the commercial software package StereoStat by RockWare ™ (see Fig. 2 to 7). In order to assess the effects of grain size on clast microfabric development within tills, the long axis data were divided into three sets: *(i)* grains < 0.25 mm in length (fine-sand and below); *(ii)* grains between 0.25 to 0.5 mm in size (medium-sand); and *(iii)* grains over > 0.5 mm in length (coarse-sand and above). The resultant data sets were plotted on a series of histograms and rose diagrams to highlight any variation in clast size versus long axis orientation.

In conjunction with the manual microstructural mapping methodology (Phillips *et al.*, 2011) an automated approach using ArcGIS line density tools was conducted on selected thin sections (X1M, Y1M, Z1M) to provide a robust, objective interpretation of the clast microfabrics. These automated tools allow the calculation of the magnitude of long axes per unit area within a thin section and was applied to each of the clast microfabrics. The variation in density (mm$^2$) of the clasts defining each microfabric was calculated with the resulting output raster files providing a map of relative intensity of clast microfabric for each thin-section (Fig. 8).

# 4. Results of the micromorphological and microstructural analysis

## *4.1. Composition and provenance of the till*

In thin section (C1M, C2M, C3M, C4M, C5M, C6M) the till is massive, lacking any obvious stratification (e.g. bedding) or other primary structure. It is composed of fine- to medium-grained, open-packed, matrix-supported, silty sand (Figs. 2-7) containing scattered, angular to well-rounded granule, to small pebble-sized rock fragments composed of sedimentary rocks (siltstone, sandstone, mudstone, indurated quartz-arenite, bioclastic limestone, micritic limestone), igneous (biotite-granite, muscovite-granite, alkali granite, micrographic intergrowth, altered volcanic rocks) and metamorphic rocks (amphibolite, biotite-schist) (Table 1). Angular to subangular, coarse-silt to sand-sized grains within the till matrix are composed of monocrystalline quartz and feldspar (plagioclase, K-feldspar). The compositional data support the conclusion of Spagnolo *et al*. (2016) that the till was laid down by ice advancing from the NW and contains far-travelled material derived from Palaeozoic sedimentary sequences within the Baltic Basin and crystalline basement rocks from Scandinavia; similar till compositions have also been reported from Germany and Denmark (Piotrowski, 1994a, b; Kjær *et al*., 2003).

The thin sections reveal that the till is compositionally, essentially homogenous with only a slight increase in the proportion of limestone and fine carbonate grains downwards through the sequence (Table 1). This increase in detrital carbonate is accompanied by the appearance of small, irregular patches of a micritic carbonate cement which appears to replace the clay within the matrix (Figs. 9a, b, c; red areas on Figs. 4 to 7). Small, rounded to irregular voids and fractures within the till are lined or filled by massive to very finely laminated, highly birefringent clay (Figs. 9d, e, f). These clay-filled features form between 5 and 15% (visual estimate) of the matrix, and locally (e.g. C1M) define a weakly developed subhorizontal “foliation”. The dark orange-brown clay is petrographically similar to clay cutan within soils, suggesting that it was deposited by water flowing through the till matrix, with the laminated nature of these fines recording several phases of fluid flow.

### *4.2. Microstructures developed in response to subglacial deformation*

Microstructural analysis of the thin sections (C1M to C6M; Figs. 2 to 7, respectively) has revealed that the tills possess five successive generations of clast microfabric (S1 to S5) defined by the preferred shape alignment of elongate coarse silt to sand-grade clasts. The relative intensity of these microfabrics varies across the thin section, reflecting the heterogeneous nature of shearing within the glacier bed. The spacing of the microfabric domains is controlled by the overall grain size of the diamicton and occurrence of coarse-sand to small pebble-sized clasts which acted as rigid bodies during deformation. Although the results of detailed microfabric analysis described below focus upon site C, comparable fabric geometries have been observed in the thin sections from sites X, Y and Z (Fig. 8).

The earliest microfabric is a very poorly developed/preserved, typically down-ice dipping S1 fabric (purple on Figs. 2 to 7). This fabric, where present, is cross-cut by a highly heterogeneous, subhorizontal to very gently inclined S2 fabric (pale green on Figs. 2 to 7). In the upper part of the till (C1M to C3M) S2 occurs within weakly to moderately well-defined, lenticular bands (Figs. 2 and 3) and is interpreted as having formed coplanar to the bed of the overriding ice. A weakly developed asymmetrical to S-shaped fabric geometry (S-C-type fabric) within the bands of S2 records a sinistral (in this plane of section) SE-directed (down-ice) sense of shear (Figs. 3, 4, 5 and 7). Lower within the till sequence (C4M to C6M), however, the banded appearance of S2 is less apparent as this fabric has been variably overprinted by a later foliation (see below).

Poorly to rarely developed, arcuate grain alignments and turbate structures (van der Meer, 1983; Menzies, 2000) occur within the microlithons between S1 and S2, and are locally truncated against these foliations. Turbate structures are interpreted to have formed where larger clasts rotate through angles up to, and greater than 360° entraining the adjacent finer grained matrix (van der Meer, 1993, 1997; Menzies, 2000; Hiemstra and Rijsdijk, 2003; Lea and Palmer, 2014). Their variable preservation within the S1 and S2 microlithons suggests that this rotational deformation occurred prior to the imposition of the clast microfabrics.

The dominant fabric is an up-ice dipping S3 microfabric (dark green on Figs. 2 to 7). This fabric cross-cuts S2, with the earlier S1 being preserved within the microlithons separating the S3 domains. In detail S3 is composed of two components: *(i)* a moderately to steeply (40° to 50°) up-ice dipping foliation; and *(ii)* a more gently inclined (20° to 40°) foliation (Figs. 2, 3 and 4). The later, down-ice dipping (20° to 40°) S4, microfabric is heterogeneous, potentially reflecting the partitioning of deformation into increasingly narrower zones of shear during the later stages of bed deformation. S2 and S3 are deformed by S4 resulting in a distinctive S-shape to sigmoidal fabric geometry comparable to an extensional crenulation cleavage (ECC fabric) associated with extensional shears formed in brittle-ductile shear zones (Passchier and Trouw, 1996). This fabric geometry once again records a sinistral, SE-directed sense of shear (Figs. 2, 3, 5 and 6) consistent with the ice movement direction in the study area (see Fig. 1c).

The same microfabric relationships (S2 to S4) were recorded in all thin sections (see Figs. 2 to 7) indicating that not only were these fabrics developed in response to the same overall stress regime, but that this regime (dominated by SE-directed shear) was maintained throughout the deposition of the entire till sequence. This conclusion is supported by the rose diagrams shown on Figs. 2 to 7 which indicate that the orientation of S2, S3 and S4 remains essentially constant throughout the till with very little modification due to compaction. The geometry of these fabrics is consistent with their development in response to the formation of Y (S2), R (S3) and P-type (S4) Reidel shears (c.f. Spagnolo *et al*., 2016) within a subhorizontal subglacial shear zone formed beneath the overriding OPIS (Fig. 10).

S1 to S4 shear related fabrics are cross-cut by a subvertical, anastomosing S5 fabric which locally wraps around the larger granule to pebble sized clasts (Figs. 3 to 7). The overall intensity of this fabric increases down-wards through the till (C2M to C6M) where it locally overprints the earlier developed foliations. The patches of micritic carbonate within the matrix of the till occur within, or close to the areas possessing a well-developed S5 fabric (Figs. 4 to 7), indicating that development of this fabric may have accompanied the passage of $CaC0_3$-bearing fluids through the sediment (see section 5).

### *4.3. Effect of grain size on microfabric development*

To assess the effects of grain size on clast microfabric development the long axis data were divided into three sets: *(i)* < 0.25mm (fine-sand and below); *(ii)* 0.25 to 0.5 mm (medium-sand); and *(iii)* > 0.5 mm in size (coarse-sand and above). The orientation data derived for these sets are shown on Figs. 11 and 12. Although the same clast microfabrics are present within all three clast sizes (Fig. 12), they are most pronounced within the finer grained components with the data highlighting a change in the orientation of the dominant fabric downwards through the till (Fig. 11). In the “upper” part of the till (C1M, C2M, C3M), the up-ice dipping S3 is dominant and its relative intensity appears to increase downwards (Figs. 11 and 12). This variation in the intensity of fabric development may record a progressive change in the relative intensity of deformation/magnitude cumulative strain imposed at the ice/bed interface during till accretion (Boulton, 1996; Boulton and Hindmarsh, 1987; Evans *et al*., 2006 and references therein). In the “lower” part of the till (C4M, C5M, C6M) the relative intensity of the shear fabrics decreases with S3 being replaced by the down-ice dipping S4 as the dominant foliation (Figs. 11 and 12). However, the fabrics (S2, S3, S4) in the "lower" part of the till have been strongly modified by the imposition of S5 (see Figs. 5 to 7). The boundary between these "upper" and "lower" till units appears to be relatively sharp and located between samples C3M and C4M. However, no obvious boundary was observed at this level within the trench (see Fig. 1c).

# 5. Variation in microfabric intensity within the OPIS till

The results of the micromorphological study indicate that there is a significant variation in the relative intensity of microfabric development within the till.

## *5.1. Automated clast microfabric analysis*

The results of the automated approach to quantify the variation in clast microfabric strength are shown in Fig. 8. The thin sections used (X1M, Y1M, Z1M) represent a traverse down the flank of an MSGL (Fig. 1c) designed to investigate any potential lateral changes in the style and relative intensity of fabric development across this subglacial landform. Importantly this method has revealed a similar pattern of microfabric development within each of the thin sections as those analysed using manual methodology of Phillips *et al*. (2011) (compare Figs. 2, 3 and 8). It is clear from Fig. 8 that all of the microfabrics (S2, S3, S4, S5) are heterogeneously developed, even within a single thin section, reflecting the partitioning of deformation on a microscale within the bed of the OPIS. S3 is the dominant fabric and is most intensely developed within the samples located close to the crest of the MSGL (X1M) and within the adjacent trough (Z1M) (Fig. 8). In contrast, both S2 and S4 are more weakly developed on top of the landform (X1M) in comparison to its flanks (Y1M, Z1M) the strength of S5 increases down the flank of the MSGL towards the adjacent trough.

## *5.2. Statistical clast microfabric analysis*

The variation in E1 eigenvalues calculated for the samples from site C (C1M to C6M) are illustrated on Fig. 13. The red colours represent areas of the thin sections with higher E1 values (0.65-0.68), corresponding to relatively stronger fabric development, and purple lower values (0.53-0.51), highlighting areas where the clast microfabrics are less well-developed. This approach reveals that fabric strength not only varies within an individual thin section, but also vertically through the till (Figs. 13 and 14a), supporting the results of the grain size fabric analysis (Figs. 11 and 12). The eigenvalues are typically higher within the upper part of the till (C1M, C2M, C3M; Table 2), recording an overall relative increase in fabric strength upwards through the till (Fig. 13); although sample C3M has the highest E1 values compared to the other two samples. In contrast, the lower three samples all possess low eigenvalues (Figs. 13 and 14a; Table 2) corresponding to much weaker fabric strengths. Although it is tempting to suggest that the lower part of the till is more weakly deformed, this may simply reflect the overprinting of the earlier shear related fabrics (S2 to S4) by the later S5 microfabric (see Figs. 5 to 7).

The eigenvalues (< 0.6; Fig. 13 and Table 2) can be used to suggest that the amount of shear being transmitted into the bed of the OPIS was relatively low. In the absence of any obvious strain markers (e.g. deformed clasts known to have been originally circular in shape) estimating the magnitude of the shear strains imparted by the overriding ice remains problematic. Several workers have used the relative abundance of selected microstructures (e.g. microshears, grain stacks) as a proxy for estimating strain in subglacial traction tills (Larsen *et al*., 2006, 2007; Narloch *et al*., 2012). However, the development of such features can be strongly lithologically controlled; e.g. microshears defined by a unistrial plasmic fabrics will only form in clay-rich sediments. Furthermore, their identification is qualitative and potentially subjective (Leighton *et al*., 2012; Neudorf *et al*., 2013). Phillips *et al*. (2013) suggested that shear strain curves established from experimental deformation studies (e.g. Thomason and Iverson, 2006) can be used to provide a minimum estimate of the shear strains experienced by subglacial traction tills. In the absence of strain curves for a range of naturally occurring tills, the potential closest "match" to the sand-rich OPIS till is the Douglas till strain curve of Thomason and Iverson (2006) (Fig. 14b). When projected onto this curve the range of average E1 values for the OPIS till suggests that microfabric development occurred in response to shear strains of < 15 (Fig. 14b). If this approach is valid then it supports the suggestion that the amount of shear being transmitted into the bed of the OPIS by the overriding ice was relatively low (cf. Larsen *et al*., 2007; Narloch *et al*., 2012; Phillips *et al*., 2013).

# 6. Implications for bed deformation beneath the OPIS

## *6.1. Foliation development in response to progressive simple shear*

Results of this detailed microscale study reveal that deformation within the bed of the OPIS was dominated by foliation development which lacked any concomitant folding and/or faulting (c.f. Spagnolo *et al*., 2016). The microfabrics define a set of up-ice and down-ice dipping Riedel shears (S3 – P-type and S4 – R-type shears; Fig. 10), as well as a subhorizontal shear foliation (S2 – Y-type shears; Fig. 10) with S2 having formed parallel to the ice-bed interface (Figs. 10 and 15). The consistency of the geometry and orientation (Figs. 2 to 7, and 15) of these microfabrics indicate that not only did subglacial deformation occur in response to the same overall stress regime, but also that they have undergone very little modification due to compaction/loading subsequent to formation which would have led to the "flattening" (decrease in dip) of the fabrics at depth within the till (see rose diagrams on Fig. 15). The consistency of the data also indicates that ductile shearing beneath the OPIS was spatially uniform and occurred within an essentially subhorizontal subglacial shear zone (see Fig. 10). Furthermore kinematic indicators (S-C and ECC-type microfabrics) record a consistent SE-directed (sinistral) sense of shear, coincident with the long axes of the MSGL and regional pattern of ice flow across the Wielkopolska Lowland (Przybylski, 2008; Spagnolo *et al*., 2016).

The cross-cutting relationships displayed by S2, S3 and S4 can be interpreted as reflecting temporal changes in the style of deformation being accommodated within the till. However, the consistent SE-directed sense of shear recorded by these fabrics clearly indicates that they formed in response to the same overall stress regime imposed during a single progressive shear event rather than completely separate phases of deformation. S2 defines a series of subhorizontal Y-type shear planes indicating that the earlier stages of ductile deformation were dominated by shear occurring coplanar to the base of the overriding ice. S2 is cross-cut by the up-ice dipping S3 foliation which defines a number of P-type shears indicating that initial layer-parallel shear was superseded by compressional deformation. S3 is then cross-cut by the later down-ice dipping S4 which records the nucleation and growth of apparently late-stage extensional R-type shears within the bed of the OPIS. The same relationships were observed in all the thin sections and are interpreted as recording temporal changes in the style of deformation imposed on the till during its evolution.

### *6.2. Clast microfabric development in tills*

The individual clast microfabrics within the OPIS till formed as a result of the passive rotation of coarse-silt to sand-grade particles into the plane of the developing foliation(s) (Fig. 16) reflecting the stress field imposed by the overriding ice (c.f. Hiemstra and Rijsdijk, 2003; Phillips *et al*., 2011). Once aligned, further rotation will cease and the clasts will maintain their preferred alignment unless there is a change in the orientation of this stress field within the evolving Reidel shears. As deformation continues, the microfabric domains defining the shear fabrics will propagate laterally as more grains become aligned. Further deformation within the microshears will be accommodated by either sliding of the grains past one another (Fig. 16a) and/or the partitioning of shear into the intervening finer grained matrix. If the matrix contains a significant modal proportion of clay minerals then this may lead to the formation of a unistrial plasmic fabric (van der Meer, 1993; Menzies, 2000; 2012; Hiemstra and Rijsdijk, 2003) coplanar to the evolving clast microfabric.

The grain size of the sediment also influenced microfabric development with preferred clast alignments being most apparent within the finer grained (< 0.25 mm; 0.25 to 0.5 mm) components (matrix) of the till (Figs. 11 and 12). During deformation, it is suggested that the larger grains (cobbles, pebbles) were the first to stop rotating, becoming “locked” into position with subsequent increments of deformation being partitioned into the still "active" matrix (c.f. Evans *et al*., 2016; Evans, 2018). Consequently the matrix of the till continued to respond to shear long after the larger clasts have become immobile and therefore provide the most complete record of subglacial deformation. Results from several micromorphological studies (Phillips *et al*., 2011, 2013, 2018) suggest that larger sand, granule to pebble sized clasts (where present) control the spacing of the developing microfabric domains, influencing the pattern of deformation partitioning within the till (Fig. 16). By the way of analogy, in metamorphic rocks the mica domains, defining the schistosity in amphibolite facies pelitic rocks (metamorphosed mudstones), are thought to nucleate upon the margins of ridged porphyroblasts (e.g. garnet), propagating laterally away from these relatively higher strain areas as deformation/fabric development continues (Bell, 1985; Bell and Rubenach, 1983; Bell *et al*., 1986; Vernon, 1989; Johnson, 1990). It is possible that a similar process also occurs in tills with the microfabrics nucleating upon the larger clasts due to the concentration of strain along the margins of these rigid grains. The evolving foliation then propagates away from this nucleation point into the adjacent matrix. The presence of larger rigid clasts will affect/distort (on a microscale) the stress and strain field imposed upon the till matrix (Fig. 16b) leading to the development of anastomosing microfabric, wrapping around these coarse sand to pebble-sized grains (Fig. 16c).

Evans *et al*. (2006) suggested that deformation (fabric development, folding, faulting) within the bed will only occur when the intergranular pore water pressure falls and a coherent "till-matrix framework" develops (also see Evans, 2018). Consequently, the nucleation and subsequent evolution of the clast microfabrics is likely to be controlled by the water content and packing of the till. However, increasing the packing of the constituent grains within the sediment will lead directly to an increase in its peak frictional strength and its resistance to deformation, which may be overcome by an increase in the magnitude of the imposed shear stress. Consequently, there is likely to be a critical range in intergranular porewater content/pressure and sediment packing for foliation development to occur within tills. For example, foliation development within a "dry" till comprising dense, closely packed grains will be limited due to the high percentage of inter granular contacts restricting grain rotation. In contrast, a shear stress applied to a water-saturated till is likely to induce dilation or even localised liquefaction which will not only inhibit fabric development, but also lead to the overprinting of earlier developed microstructures (Evans *et al*., 2006; Phillips *et al*., 2011; 2013; 2018). The inherent spatial variation in the water content and packing of the till will lead to the small-scale partitioning of deformation and heterogeneous fabric development within the bed of the OPIS (Figs. 2 to 8).

### *6.3. Evidence of intergranular fluid flow and dewatering of the bed*

The matrix of the till forming the bed of the OPIS contains clay-lined or filled voids, intergranular pore spaces and fractures (Fig. 9). The clay is petrographically similar to clay cutan within soils, suggesting that it was deposited by water flowing through the till so that the laminated nature of these fines records several phases of fluid flow. Although clay infiltration can occur during pedogenic processes, these features occur well below the base of the modern soil (see Fig. 1d) indicating that it was unrelated to recent pedogenic processes. Observations from contemporary (Alley *et al*., 1986; Tulaczyk *et al.,* 1998) and palaeo (Ó Cofaigh *et al*., 2007) ice stream beds indicate that the tills are typically highly porous and weak, with a water content close to the liquid limit. The clay within the OPIS till forms between 5 and 15 % of the matrix and is observed variably infilling intergranular pore spaces, consistent with the nature of tills described from modern ice stream beds (Alley *et al*., 1986; Tulaczyk *et al.,* 1998; Ó Cofaigh *et al*., 2007). Significant compaction of the OPIS till would have led to an increase in its packing, reducing in its porosity and permeability. Consequently the preferred interpretation is that fluid flow and clay infiltration probably occurred shortly after till deposition; a conclusion supported by the dark coloration of the clay resulting from its replacement by Fe/Mn during 'maturation' (van der Meer, 2007 pers. comm.; Phillips and Auton, 2008).

In the lower part of the OPIS till the earlier shear fabrics (S2 to S4) are variably overprinted by S5 (Fig. 15). The intergranular clays show very little, if any, evidence of disruption/fragmentation suggesting that they post-date any significant deformation and/or reorganisation of the structure and packing of the till during the imposition of S5. Consequently, it is suggested that S5 pre-dated the intergranular fluid flow and clay infiltration, with the imposition of this late stage foliation probably accompanying the dewatering of the till driven by the ice overburden pressure; a conclusion supported by the relative increase in the intensity of this fabric downward through the till (Fig. 15). The micritic carbonate within the matrix of the till (red areas on Fig. 15) exhibits a close spatial relationship to S5, indicating that diagenesis may have accompanied the imposition of this fabric and recording the passage of a $CaCO_3$-bearing fluid phase through the sediment. If the carbonate was pedogenic then it should increase upwards towards the base of the modern soil, possibly forming a calcified crust at the base of the soil profile. Several studies have examined the dissolution of carbonate in glacial environments (e.g. Fairchild *et al*., 1993; 1994; Menzies and Brand, 2007) with McGillen and Fairchild (2005) suggesting that this process may be facilitated by the crushing and comminution of carbonate grains within subglacial traction tills. Menzies and Brand (2007) argued that carbonate cementation of ice-contact sands and gravels exposed within core of a large drumlin in New York State occurred in response to a reduction in hydrostatic pressure and release of $CO_2$ from the meltwater escaping from beneath the Laurentide Ice Sheet. Consequently, it is possible that carbonate diagenesis within the OPIS till may have occurred penecontemporaneous with subglacial deformation. As noted above, S5 clearly overprints the shear related fabrics within the till and therefore post-dated subglacial shearing. However, due to the potentially diachronous nature of deformation within the OPIS till, dewatering and imposition of S5 within the structural lower parts of the sequence is thought to have been initiated whilst subglacial shearing was continuing at a higher level within the bed (Fig. 15) (see below).

### *6.4. The nature of bed deformation beneath the OPIS: deformation partitioning or incremental progressive simple shear during till accretion*

Spagnolo *et al*. (2016) argued that the till beneath the OPIS was being continuously accreted at the top of a shallow-deforming bed (cf. Tulaczyk, 1999; Iverson *et al*., 1998; Fuller and Murray, 2000; Piotrowski *et al*., 2001, 2004; Evans *et al*., 2006; Cuffey and Paterson, 2010; Iverson, 2011; Evans, 2018). However, the possibility that pervasive bed deformation may have occurred to greater depths beneath this ice stream needs to be considered. Quantitative data presented here provides evidence that fabric (S2, S3, S4, S5) strength varies (on a microscale) both laterally and vertically within the bed of the OPIS (Figs. 13 and 15). If this variation in fabric strength can be used as a proxy for the relative intensity of shear imposed on the till it may reflect either: *(i)* the partitioning of deformation within the subglacial shear zone formed beneath this ice stream, within the deforming bed and potentially encompassing the entire thickness of the till; or *(ii)* the variation in the magnitude of the shear being transmitted into the deforming bed during the progressive accretion of the OPIS till.

A number of studies have suggested that subglacial shear zones migrate through the bed due to spatial and temporal fluctuations in water content/pressure (Tulaczyk, 1999; Truffer *et al*., 2000; Evans *et al*., 2006; Kjær *et al*., 2006; Lee and Phillips, 2008) and/or the ability of these sediments to drain intergranular porewater (Piotrowski *et al*., 2004). Deformation within the shear zone can either be 'pervasive' (homogeneous) and transmitted throughout the entire bed (van der Meer *et al*., 2003; Menzies *et al*., 2006), or heterogeneous where the bed comprises a 'mosaic' of actively deforming and stable (non-deforming) zones (Piotrowski and Kraus, 1997; Piotrowski *et al*., 2004; Lee and Phillips, 2008). Tills within the beds of ice streams are thought to be water-saturated and weak (Alley *et al*., 1986; Tulaczyk *et al*., 1998; Ó Cofaigh *et al*., 2007), and therefore able to accommodate a significant proportion of the forward motion of the overriding ice. The consistency of the orientation and geometry of the shear fabrics (S2 to S4; Fig. 15) throughout the OPIS till, coupled with the very low preliminary estimates of shear strain (Fig. 14) may be used to support the presence of weak, water-saturated sediments beneath this palaeo-ice stream, facilitating the transmission of shear throughout its entire bed (Hart and Boulton, 1991; van der Wateren *et al*., 2000; van der Meer *et al*., 2003; Menzies *et al*., 2006). In detail, the relative intensity of the shear fabrics vary both laterally and vertically (Figs. 8 and 13). However, there is no obvious macroscale evidence for the presence of a significant décollement surface (thrust) within the bed of the OPIS till (see Fig. 1d). So as a result, it cannot be argued that forward motion of the OPIS was accommodated by deformation at a deeper level within the sediment pile (Fig. 17a). Consequently, variations in the relative intensity of foliation development within the OPIS till is more likely to record the small-scale partitioning of deformation during subglacial shear.

The deforming bed model for glacier motion predicts an increase in cumulative strain upwards toward the ice-bed interface (Boulton, 1986; Boulton and Hindmarsh, 1987; Evans *et al*., 2006) with deformation being accommodated by a weak, water-saturated layer located immediately adjacent to, or at the ice-bed interface (Fig. 17b). The continuous deposition of a soft (weak), compositionally homogenous (well-mixed; see section 4.1) till layer at the top of the bed of the OPIS (Spagnolo *et al*., 2016) means that over time deformation will have progressively shifted upwards as till accreted (Fig. 17b). The trenches in the study area reveal that the till sequence beneath the OPIS is at least 1.2 to 1.4 m thick, with Ground Penetrating Radar data indicating that the diamicton may be in the order of 2 to 3 m thick (Spagnolo *et al*., 2016). The soft deforming layer responsible for till accretion at the top of this sequence is likely to have only been a few tens of centimetres thick (Menzies 1982; Alley *et al*., 1986, 1987; Boulton, 1996; Hindmarsh, 1998; Larsen *et al*., 2004, 2007; Evans *et al*., 2006; Stokes *et al*., 2013a) and localised in nature reflecting the spatial and temporal changes in bed conditions. Phillips *et al*. (2018) suggested that the term 'transient mobile zone' for this actively deforming layer in order to emphasize the spatial and temporal variations in subglacial deforming bed processes proposed by a number of researchers (e.g. Piotrowski and Kraus, 1997; Boyce and Eyles, 2000; van der Meer *et al*., 2003; Larsen *et al*., 2004, 2007; Piotrowski *et al*., 2004, 2006; Evans *et al*., 2006; Meriano and Eyles, 2009; Evans, 2018). The focusing of deformation into this water-saturated mobile layer would have effectively switched off deformation at a deeper level within the bed. As a consequence of this progressive till accretion-deformation, the relative age of subglacial shearing beneath the OPIS would be diachronous, becoming progressively younger toward the top of the bed. The observed vertical variation in the relative intensity of the shear fabrics (S2 to S4; Figs. 13 and 15) may therefore be interpreted as recording changes in the magnitude of the cumulative strain being recorded by the till during this accretion-deformation process (Fig. 17c) (cf. Larsen *et al*., 2004). The variation in fabric strength may reflect the degree of coupling between the ice and the underlying bed; the greater the fabric intensity the higher the degree of ice-bed coupling and transmission of shear into the bed.

Preliminary estimates of the shear strains involved are low (< 15; Fig. 14b) indicating that the amount of shear being transmitted into the bed of the OPIS was relatively small (cf. Larsen *et al*., 2006; Narloch *et al*., 2012; Phillips *et al*., 2013). Consequently, fast flow of this ice stream would have been largely accommodated by either basal sliding and/or flow deformation within a weak, water-saturated layer located at the top of the accreting till sequence (Evans *et al*., 2006; Phillips *et al*., 2013; Spagnolo *et al*., 2016). Evidence of the latter is potentially provided by the rotational turbate structures (van der Meer, 1993, 1997; Menzies, 2000; Hiemstra and Rijsdijk, 2003). These structures are truncated by the shear fabrics, indicating that rotational deformation occurred prior to foliation development within the OPIS till. Turbate structures form where larger clasts are able to rotate through angles of up to, or > 360°, entraining the adjacent finer grained matrix (van der Meer, 1993; Menzies, 2000; Lachniet *et al*., 2001; Hiemstra and Rijsdijk, 2003; Phillips, 2006; Lea and Palmer, 2014). This requires either very high shear strains or the lowering of the strength of the sediment enabling clast rotation at the much lower strains (Evans *et al*., 2006), the latter being more likely due to the very low shear strain estimates obtained for the OPIS till. The presence of an active layer at the top of the bed would have markedly reduced or even prevented transmission of the shear into the underlying till. Furthermore, this layer is likely to have been highly mobile, facilitating the advection of well-mixed, far-travelled sediment down-ice and the continuous accretion of till at the top of a shallow deforming bed (Spagnolo *et al*., 2016). Spatial and temporal fluctuations in the water content within this active layer will have affected the degree of ice-bed coupling, leading to the observed complex pattern of cumulative strain (Figs. 13, 14 and 15).

Microtextural evidence (sections 5 and 6) indicates dewatering, consolidation and cementation of the OPIS till. These processes could have led to an increase in the shear strength of the till potentially resulting in the increased “stabilisation” of the sediment within the cores of the MSGL as they grew beneath the OPIS. Till consolidation or the presence of a relatively hard/stiff core has been invoked in the initiation of some subglacial landforms (e.g. Menzies and Brand 2007; Menzies *et al*., 2016), although this concept is challenged by the regular spatial distribution of these landforms (e.g. Spagnolo *et al*., 2016). In specific case presented here, the results suggest that till consolidation may have been initiated at a lower level within the MSGL whilst till deformation and accretion continued above (see sections 6.3. and 6.4), thus providing no support for the idea that a stiffened core is required for MSGL initiation.

Although it is acknowledged that the detailed micromorphological/microstructural study presented here has largely focused upon a single site (site C), the results are applicable to the wider footprint of the OPIS as well as other contemporary and palaeo-ice streams. Deformation beneath glaciers and ice sheets is widely viewed as being dominated by simple shear within a subglacial shear zone (e.g. van der Wateren *et al*., 2000; Hart, 2007; Lee and Phillips, 2008; Benn and Evans 2010). The style of deformation identified within the bed of the OPIS is consistent with this assumption, with comparable microscale shear fabrics being recognised in subglacial traction tills (sensu Evans *et al*., 2006) from other glaciated terrains (e.g. Germany - van der Wateren *et al*., 2000; England (Norfolk) - Vaughan-Hirsh *et al*., 2013; British Columbia, Canada - Neudorf *et al*., 2013; Central Poland - Narloch *et al*., 2012, 2013; Baltic Coast, northern Germany - Brumme, 2015; Gehrmann *et al*., 2017; Scotland - Phillips *et al*., 2011, 2018; Switzerland - Phillips *et al*., 2013). In structural geology, Pumpelly's rule states that small deformation structures are a key to understanding the structural evolution of an area as they mimic the styles and orientations of a larger-scale structures of the same generation. Consequently, the geometry and the relationships displayed between the range of microscale (and macro-) structures found within subglacially deformed sediments can not only be used to establish the overall stress regime responsible for deformation (e.g. van der Wateren *et al*., 2000; Vaughan-Hirsh *et al*., 2013; Gehrmann *et al*., 2017), but also aid in the reconstruction of the regional pattern of ice movement (e.g. Brumme, 2015). The bed of the OPIS across the Wielkopolska Lowland region is very gently undulating (Fig. 1c) (Przybylski, 2008; Spagnolo *et al*., 2016) and can, in general, be considered to be represented by an essentially subhorizontal ductile-brittle shear zone. The thick (c. 30 m) sequence of Quaternary sediments which blanket the area result in an absence of any major bedrock highs which would have imposed significant changes on the stress regime active within the bed of this palaeo-ice stream. Furthermore, gravel to cobble-sized clasts, which would have locally influenced (modified) microscale fabric development, are rare with the OPIS till. Consequently, the proposed model of progressive ductile shearing during till accretion is considered to be applicable across the bed of the Odra palaeo-ice stream with changes in microfabric geometry reflecting local changes in the physical properties of the sediment (e.g. grain size, porewater content) during fast ice flow.

# 7. Conclusions

The detailed microstructural study of the thick subglacial traction till formed within the bed of the Weichselian Odra palaeo-ice stream contributes to our understanding of the deformation processes occurring within its bed and it how it evolved over time.

- The massive, compositionally homogenous nature of the till indicates that the sediment being accreted to the bed was well-mixed and included far travelled material derived from Palaeozoic rocks of the Baltic Basin and crystalline basement of Scandinavian, consistent with the till being laid down by ice advancing from the NE.

- Deformation within the bed of the ice stream was dominated by foliation development (S1 to S5) recording progressive ductile shearing within a subhorizontal subglacial shear zone. Cross-cutting relationships displayed by these shear fabrics (S2, S3 and S4) reflect temporal changes in the style of deformation being accommodated within the till during a single progressive shear event as the till accreted vertically. Kinematic indicators (S-C and ECC-type microfabrics) within the till record a consistent SE-directed (sinistral) sense of shear coincident with the regional pattern of ice flow across the Wielkopolska Lowland.
- The clast microfabrics reflect the stress field imposed by the overriding ice and form as a result of the passive rotation of detrital grains into the plane of the developing foliation(s). Larger clasts (pebbles, cobbles) become "locked" into position at an earlier stage within the deformation history and with subsequent shear being partitioned into the matrix of the till. These larger clasts then control the partitioning of deformation within the till and the spacing of the evolving microfabric domains.
- Evidence of intergranular pore water flowing through the bed of the OPIS is provided by the presence of clay-filled pore spaces within the till matrix having potentially occurred during or shortly after deposition. Further evidence of fluid flow through the bed is provided by the anastomosing, subvertical S5 fabric which formed in response to the dewatering and consolidation of the till in response to deposition from the deforming layer and final shutdown of the ice stream. Dewatering of the bed was accompanied by the growth of diagenetic micritic carbonate indicating that the escaping fluid contained dissolved $CaC0_3$ derived from the dissolution of detrital limestone.
- Bed deformation beneath the OPIS occurred in response to incremental progressive simple shear during till accretion. The relative age of deformation was diachronous (younger towards the top of the bed) as a thin deforming layer migrated progressively upwards in response to till accretion at the top of the ice stream bed. Focusing of deformation into this "active" layer or "transient mobile zone" effectively switched off deformation deeper within the bed. Variations in the relatively intensity of the microfabrics may record changes in the magnitude of the cumulative strain being imposed on the till during this accretion-deformation process and the degree of coupling between the ice and the underlying bed. Preliminary estimates of the shear strains involved are low, indicating that the amount of shear being transmitted into the bed of the OPIS was relatively small. This has implications for the mechanism responsible for the forward motion of this palaeo-ice stream.

## 8. Acknowledgements

The authors would like to thank various colleagues for numerous discussions on the nature of glacier bed deformation over the years, in particular Dave Evans, Jaap van der Meer, Jonathan Lee, Clive Auton, Jon Merritt, Chris Clark, Chris Stokes, Wojciech Wysota, Iza Szuman and Adriano Ribolini. Adrian Palmer (Royal Holloway University of London) is thanked for his expertise in making the thin sections. David J.A. Evans and one anonymous reviewer are thanked for their constructive reviews of this paper. ERP publishes with the permission of the Executive Director of the British Geological Survey, Natural Environmental Research Council.

## 9. References

Alley, R.B., 1989. Water pressure coupling of sliding and bed deformation: 1. Water system. Journal of Glaciology 35, 108-118.

Alley, R.B., Blankenship, D.D., Bentley, C.R., Rooney, S.T., 1986. Deformation of till beneath ice stream B, West Antarctica. Nature 322, 57-59.

Alley, R.B., Blankenship, D.D., Bentley, C.R., Rooney, S.T., 1987a. Till beneath ice stream B: 3. Till deformation: evidence and implications. Journal of Geophysical Research 92, 8921-8929.

Alley, R.B., Blankenship, D.D., Rooney, S.T., Bentley, C.R., 1987b. Till beneath ice stream B: 4. A coupled ice-till flow model. Journal of Geophysical Research 92, 8931-8940.

Bamber, J.L., Vaughan, D.G., Joughin, I., 2000. Widespread complex flow in the interior of the Antarctic Ice Sheet. Science 287, 1248–1250.

Baroni, C., Fasano, F., 2006. Micromorphological evidence of warm-based glacier deposition from the Ricker Hills Tillite (Victoria Land, Antarctica). Quaternary Science Reviews. 25, 976-992.

Bell, T.H., 1985. Deformation partitioning and porphyroblast rotation in metamorphic rocks: a radical reinterpretation. Journal of Metamorphic Geology 3, 109-118.

Bell, T.H., Rubenach, M.J., 1983. Sequential porphyroblast growth and crenulation cleavage development during progressive deformation. Tectonophysics 92, 171-194.

Bell, T.H., Rubenach, M.J., Fleming, P.D., 1986. Porphyroblast nucleation, growth and dissolution in regional metamorphic rocks as a function of deformation partitioning during foliation development. Journal of Metamorphic Geology 4, 37-67.

Bennett, M.R., 2003. Ice streams as the arteries of an ice sheet: their mechanics, stability and significance. Earth Science Reviews 61, 309–339.

Bingham, R.G., Vaughan, D.G., King, E.C., Davies, D., Cornford, S.L., Smith, A.M., Arthern, R.J., Brisbourne, A.M., Rydt, J., Graham, A.G., Spagnolo, M., 2017. Diverse landscapes beneath Pine Island Glacier influence ice flow. Nature communications 8, 1618.

Boulton, G.S., 1996. Theory of glacial erosion, transport and deposition as a consequence of subglacial deformation. Journal of Glaciology 42, 43-62.

Boulton, G.S., Hindmarsh, R.C.A., 1987. Sediment deformation beneath glaciers: rheology and geological consequences. Journal of Geophysical Research 92, 9059-9082.

Boulton, G.S., Dobbie, K.E., Zatsepin, S., 2001. Sediment deformation beneath glaciers and its coupling to the subglacial hydraulic system. Quaternary International 86, 3-28.

Boyce, J.I., Eyles, N., 2000. Architectural element analysis applied to glacial deposits: internal geometry of a late Pleistocene till sheet, Ontario, Canada. Bulletin of the Geological Society of America 112, 98-118.

Brumme, J., 2015. Three-dimensional microfabric analyses of Pleistocene tills from the cliff section Dwasieden on Rügen (Baltic Sea coast): micromorphological evidence for subglacial polyphase deformation (PhD thesis). Ernst-Moritz-Arndt-Universitstäat, Greifswald, 210pp.

Clarke, G.K.C., 1987. Subglacial till: a physical framework for its properties and processes. Journal of Geophysical Research 92, 9023-9036.

Cuffey, K.M., Paterson, W.S.B., 2010. The Physics of Glaciers Fourth Edition. Academic Press, Oxford.

Denis, M., Guiraud, M., Konaté, M., Buoncristiani, J.-F., 2010. Subglacial deformation and water-pressure cycles as a key for understanding ice stream dynamics: evidence from the Late Ordovician succession of the Djado Basin (Niger). International Journal of Earth Science (Geol Rundsch) 99, 1399-1425.

Dyke, A.S., Morris, T.F., 1988. Drumlin fields, dispersal trains, and ice streams in Arctic Canada. Canadian Geographer 32, 86–90.

Evans, D.J., Phillips, E.R., Hiemstra, J.F., Auton, C.A., 2006. Subglacial till: formation, sedimentary characteristics and classification. Earth Science Reviews 78, 115-176.

Evans, D.J.A., Roberts, D.H., Evans, S.C., 2016. Multiple subglacial till deposition: A modern exemplar for Quaternary palaeoglaciology. Quaternary Science Reviews 145, 183-203.

Evans, D.J.A., 2018. Till: A Glacial Process Sedimentology. John Wiley and Sons Ltd, UK.

Fairchild, I.J., Bradby, L., Spiro, B., 1993. Carbonate diagenesis in ice. Geology 21, 901-904.

Fairchild, I.J., Bradby, L., Spiro, B., 1994. Reactive carbonate in glacial systems: a preliminary synthesis of its creation, dissolution and reincarnation. In Deymoux, M., Miller, J.M.G., Domack, E.W., Young, G.M. (Eds) International Geological Correlation Project 260: Earth's Glacial record. Cambridge University Press. 176-192.

Fuller, S., Murray, T., 2002. Sedimentological investigations in the forefield of an Icelandic surge-type glacier: implications for the surge mechanism. Quaternary Science Reviews 21, 1503-1520.

Gehrmann, A., Hüneke, H., Meschede, M., Phillips, E. 2017. 3D microstructural architecture of deformed glacigenic sediments associated with large-scale glacitectonism, Jasmund Peninsula (NE Rügen), Germany. Journal of Quaternary Science 32, 213-230. DOI: 10.1002/jqs.2843.

Hart, J.K., Boulton, G.S., 1991. The interrelation of glaciotectonic and glaciodepositional processes within the glacial environment. Quaternary Science Reviews 10, 335-350.

Hiemstra, J.F., van der Meer, J.J.M., 1997. Pore-water controlled grain fracturing as an indicator for subglacial shearing in tills. Journal of Glaciology 43, 446-454.

Hiemstra, J.F., Rijsdijk, K.F. 2003. Observing artificially induced strain: implications for subglacial deformation. Journal of Quaternary Science 18, 373-383.

Hiemstra, J.F., Rijsdijk, K.F., Evans, D.J.A., van der Meer, J.J.M., 2005. Integrated micro- and macro-scale analyses of Last Glacial maximum Irish Sea diamicts from Abermaw and Treath y Mwnt, Wales, UK. Boreas 34, 61-74.

Hindmarsh, R.C.A., 1998b. The stability of a viscous till sheet coupled with ice flow, considered at wavelengths less than the ice thickness. Journal of Glaciology 44, 285-292.

Hindmarsh, R.C., 2009. Consistent generation of ice-streams via thermo-viscous instabilities modulated by membrane stresses. Geophysical Research Letters 36(6).

Hodgson, D.A., 1994. Episodic ice streams and ice shelves during retreat of the northwestern most sector of the Late Wisconsinan Laurentide Ice Sheet over the central Canadian Arctic archipelago. Boreas 23, 14-28.

Humphrey, N., Kamb, B., Fahnestock, M., Engelhardt, H., 1993. Characteristics of the bed of the lower Columbia Glacier, Alaska. Journal of Geophysical Research 98, 837-846.

Iverson, N.R., 2011. Shear resistance and continuity of subglacial till: hydrology rules. Journal of Glaciology 56, 1104-1114.

Iverson, N.R., Hooyer, T.S., Baker, R.W. 1998. Ring-shear studies of till deformation: Coulomb-plastic behaviour and distributed strain in glacier beds. Journal of Glaciology 44, 634-642.

Johnson, S.E. 1990. Lack of porphyroblast rotation in the Otago schists. New Zealand: implications for crenulation cleavage development, folding and deformation partitioning. Journal of Metamorphic Geology 8, 13-30.

King, E.C., Hindmarsh, R.C., Stokes, C.R., 2009. Formation of mega-scale glacial lineations observed beneath a West Antarctic. Nature Geoscience 2, 585–588.

Kjaer, K.H., Houmark-Nielsen, M., Richardt, N., 2003. Ice-flow patterns and dispersal of erratics at the southwestern margin of the last Scandinavian Ice Sheet: signature of palaeo-ice streams. Boreas 32, 130-148.

Kjær, K.H., Larsen, E., van der Meer, J.J.M., Ingólfsson, Ó., Krüger, J., Benediktsson, I.Ó., Knudsen, C.G., Schomacker, A., 2006. Subglacial decoupling at the sediment/bedrock interface: a new mechanism for rapid flowing ice. Quaternary Science Reviews 25, 2704-2712.

Khatwa, A., Tulaczyk, S., 2001. Microstructural interpretations of modern and Pleistocene subglacially deformed sediments: the relative role of parent material and subglacial processes. Journal of Quaternary Science 16, 507-517.

Kozarski, S., 1988. Time and dynamics of the last Scandinavian ice-sheet retreat from northwestern Poland. Geographica Polonica 55, 91-101.

Kyrke-Smith, T.M., Katz, R.F., Fowler, A.C., 2015. Subglacial hydrology as a control on emergence, scale, and spacing of ice streams. Journal of Geophysical Research: Earth Surface 120, 1501-1514.

Lachniet, M.S., Larson, G.J., Lawson, D.E., Evenson, E.B., Alley, R.B., 2001. Microstructures of sediment flow deposits and subglacial sediments: a comparison. Boreas 30, 254-262.

Larsen, N. K., Piotrowski, J. A. and Kronborg, C. 2004. A multiproxy study of a basal till: a time-transgressive accretion and deformation hypothesis. Journal of Quaternary Science 19, 9–21

Larsen, N.K., Piotrowski, J.A., Christiansen, F., 2006. Microstructures and micro-shears as proxy for strain in subglacial diamicts: implications for basal till formation. Geology. 34, 889-892.

Larsen, N.K., Piotrowski, J.A., Menzies, J., 2007. Microstructural evidence of low-strain, time transgressive subglacial deformation. Journal of Quaternary Science. 22, 593-608.

Lea, J.M., Palmer, A., 2014. Quantification of turbate microstructures through a subglacial till: dimensions and characteristics. Boreas. 10.1111/bor.12073. ISSN 0300-9483.

Lee, J.R., Phillips, E.R., 2008. Progressive soft sediment deformation within a subglacial shear zone – a hybrid mosaic-pervasive deformation model for Middle Pleistocene glaciotectonised sediments from eastern England. Quaternary Science Reviews 27, 1350-1362.

Leighton, I.D., Hiemstra, J.F., Weidman, C.T., 2012. Recognition of micro-scale deformation structures in glacial sediments – pattern perception, observer bias and the influence of experience. Boreas, 10.1111/j.1502-3885.2011.00246.x. ISSN 0300-9483.

McGillen, M.R., Fairchild, I.J., 2005. An experimental study of incongruent dissolution of $CaCO_3$ under analogue glacial conditions. Journal of Glaciology 51, 383-390.

Marks, L., 2012. Timing of the Late Vistulian (Weichselian) glacial phases in Poland. Quaternary Science Reviews 44, 81-88.

Margold, M., Stokes, C.R., Clark, C.D. 2015. Ice Streams in the Laurentide Ice Sheet: Identification, characteristics and comparison to modern ice sheets. Earth-Science Reviews 143, 117-146.

Menzies, J., 1982. Till hummock (proto-drumlin) at the ice glacier bed interface. In: Davidson-Arnott, R., Nickling, W., Fahey, B.D. (Eds.), Research in Glacial, Glacio-Fluvial and Glacio-Lacustrine Systems. Proceedings of the 6th Guelph Symposium on Geomorphology, 33-47.

Menzies, J., 2000. Micromorphological analyses of microfabrics and microstructures indicative of deformation processes in glacial sediments. In: A.J. Maltman, B. Hubbard, M.J. Hambrey (eds.). Deformation of glacial materials. Geological Society of London, Special Publication 176, 245-257.

Menzies, J., 2012. Strain pathways, till internal architecture and microstructures – perspectives on a general kinematic model – a 'blueprint' for till development. Quaternary Science Reviews 50, 105-124.

Menzies, J., Maltman, A.J., 1992. Microstructures in diamictons - evidence of subglacial bed conditions. Geomorphology 6, 27-40.

Menzies, J., Brand, U., 2007. The internal sediment architecture of a drumlin, Port Byron, New York State, USA. Quaternary Science Reviews 26, 322-335.

Menzies, J., Zaniewski, K., Dreger, D., 1997. Evidence from microstructures of deformable bed conditions within drumlins, Chimney Bluffs, New York State. Sedimentary Geology 111, 161-175.

Menzies, J., van der Meer, J.J.M., Rose, J., 2006. Till – a glacial "tectomict", a microscopic examination of a till's internal architecture. Geomorphology 75, 172-200.

Menzies, J., Hess, D.P., Rice, J.M., Wagner, K.G., Ravier, E., 2016. A case study in the New York Drumlin Field, an investigation using microsedimentology, resulting in the refinement of a theory of drumlin formation. Sedimentary Geology 338, 84-96.

Meriano, M., Eyles, N., 2009. Quantitative assessment of the hydraulic role of subglaciofluvial interbeds in promoting deposition of deformation till (Northern Till, Ontario). Quaternary Science Reviews 28, 608-620.

Narloch, W., Piotrowski, J.A., Wysota, W., Larsen, N.K., Menzies, J., 2012. The signature of strain magnitude in tills associated with the Vistula Ice Stream of the Scandinavian Ice Sheet, central Poland. Quaternary Science Reviews 57, 105-120.

Narloch, W., Wysota, W., Piotrowski, J.A., 2013. Sedimentological record of subglacial conditions and ice sheet dynamics of the Vistula Ice Stream (north-central Poland) during the Last Glaciation. Sedimentary Geology 293, 30-44.

Neudorf, C. M., Brennand, T. A., Lian, O. B., 2013. Till-forming processes beneath parts of the Cordilleran Ice Sheet, British Columbia, Canada: macroscale and microscale evidence and a new statistical technique for analysing microstructure data. Boreas, 10.1111/bor.12009. ISSN 0300-9483.

O´ Cofaigh, C., Evans, J., Dowdeswell, J.A., Larter, R. 2007. Till characteristics, genesis and transport beneath Antarctic paleo-ice streams. Journal of Geophysical Research 112, F03006.

Palmer, A.P. 2005. The micromorphological description, interpretation and palaeoenvironmental significance of lacustrine clastic laminated sediments. Unpublished PhD thesis, University of London.

Passchier, C.W., Trouw, R.A.J., 1996. Microtectonics. Springer.

Patterson, C.J., 1997. Southern Laurentide ice lobes were created by ice streams: Des Moines Lobe in Minnesota, USA. Sedimentary Geology 111, 249-261.

Patterson, C.J., 1998. Laurentide glacial landscapes: the role of ice streams. Geology 26, 643-646.

Phillips, E.R., 2006. Micromorphology of a debris flow deposit: evidence of basal shearing, hydrofracturing, liquefaction and rotational deformation during emplacement. Quaternary Science Reviews 25, 720-738.

Phillips, E., Merritt, J.W., Auton, C.A., Golledge, N.R., 2007. Microstructures developed in subglacially and proglacially deformed sediments: faults, folds and fabrics, and the influence of water on the style of deformation. Quaternary Science Reviews 26, 1499-1528.

Phillips, E.R., Auton, C.A., 2000. Micromorphological evidence for polyphase deformation of glaciolacustrine sediments from Strathspey, Scotland. In: Maltman, A.J., Hubbard, B., Hambrey, M.J. (Eds). Deformation of glacial materials. The Geological Society of London, Special Publication 176, 279-291.

Phillips, E.R., Auton, C.A., 2008. Microtextural analysis of a glacially 'deformed' bedrock: implications for inheritance of preferred clast orientations in diamictons. Journal of Quaternary Science 23, 229-240.

Phillips, E., Merritt, J., 2008. Evidence for multiphase water-escape during rafting of shelly marine sediments at Clava, Inverness-shire, NE Scotland. Quaternary Science Reviews 27, 988–1011.

Phillips, E.R., van der Meer, J.J.M., Ferguson, A., 2011. A new ‘microstructural mapping’ methodology for the identification and analysis of microfabrics within glacial sediments. Quaternary Science Reviews 30, 2570-2596.

Phillips, E., Everest, J., Reeves, H., 2013. Micromorphological evidence for subglacial multiphase sedimentation and deformation during overpressurized fluid flow associated with hydrofracturing. Boreas 42, 395–427.

Phillips, E.R., Lipka, E., van der Meer, J.J.M. 2013. Micromorphological evidence of liquefaction and sediment deposition during basal sliding of glaciers. Quaternary Science Reviews 81, 114-137.

Phillips, E., Evans, D.J.A., van der Meer, J.J.M., Lee, J.R. 2018. Microscale evidence of liquefaction and its potential triggers during soft-bed deformation within subglacial traction tills. Quaternary Science Reviews 181, 123-143.

Piotrowski, J.A., 1994a. In Warren, W.P., Croot, D. (eds) Formation and Deformation of Glacial Deposits, Balkema, Rotterdam. 3-8.

Piotrowski, J.A., 1994b. Tunnel-valley formation in northwest Germany—geology, mechanisms of formation and subglacial bed conditions for the Bornhöved Tunnel Valley. Sedimentary Geology 89, 107-141.

Piotrowski, J.A., Kraus, A.M., 1997. Response of sediment to ice sheet loading in northwestern Germany: effective stresses and glacier bed stability. Journal of Glaciology 43, 495-502.

Piotrowski, J.A., Tulaczyk, S., 1999. Subglacial conditions under the last ice sheet in northwest Germany: ice-bed separation and enhanced basal sliding? Quaternary Science Reviews 18, 737-751.

Piotrowski, J.A., Mickelson, D.M., Tulaczyk, S., Krzyszowski, D., Junge, F. 2001. Were subglacial deforming beds beneath past ice sheets really widespread? Quaternary International 86, 139-150.

Piotrowski, J.A., Larsen, N.K., Junge, F., 2004. Soft subglacial beds: a mosaic of deforming and stable spots. Quaternary Science Reviews 23, 993-1000.

Piotrowski, J.A., Larsen, N.K., Menzies, J., Wysota, W., 2006. Formation of subglacial till under transient bed conditions: deposition, deformation, and basal decoupling under a Weichselian ice sheet lobe, central Poland. Sedimentology 53, 83-106.

Przybylski, B., 2008. Geomorphic traces of a Weichselian ice stream in the Wielkopolska Lowland, western Poland. Boreas 37, 286-296.

Spagnolo, M., Clark, C.D., Ely, J.C., Stokes, C.R., Anderson, J.B., Andreassen, K., Graham, A.G.C., King, E.C., 2014. Size, shape and spatial arrangement of mega-scale glacial lineations. Earth Surface Processes and Landforms 39, 1432-1448.

Spagnolo, M., Phillips, E., Piotrowski, J.A., Rea, B.R., Clark, C.D., Stokes, C.R., Carr, S.J., Ely, J.C., Adriano Ribolini, A., Wysota, W., Izabela Szuman, I., 2016. Ice stream motion facilitated by a shallow-deforming and accreting bed. Nature Communications DOI: 10.1038/ncomms10723.

Spagnolo, M., Bartholomaus, T.C., Clark, C.D., Stokes, C.R., Atkinson, N., Dowdeswell, J.A., Ely, J.C., Graham, A., Hogan, K.A., King, Larter, R.D., E., Livingstone, S.J., Pritchard. H.D., 2017. The periodic topography of ice stream beds: insights from the Fourier spectra of mega-scale glacial lineations. Journal of Geophysical Research: Earth Surface 122, 1355-1373.

Stokes, C.R., Clark, C.D., 1999. Geomorphological criteria for identifying Pleistocene ice streams. Annals of Glaciology 28, 67-75.

Stokes, C.R., Clark, C.D., 2001. Palaeo-ice streams. Quaternary Science Reviews 20, 1437-1457.

Stokes, C.R., Clark, C.D., 2002. Are long subglacial bedforms indicative of fast ice flow? Boreas 31, 239-249.

Stokes, C.R., Clark, C.D., 2003. The Dubawnt Lake palaeo-ice stream: evidence for dynamic ice sheet behaviour on the Canadian Shield and insights regarding the controls on ice stream location and vigour. Boreas 32, 263-279.

Stokes, C.R., Fowler, A.C., Clark, C.D., Hindmarsh, R.C.A., Spagnolo, M., 2013a. The instability theory of drumlin formation and its explanation of their varied composition and internal structure. Quaternary Science Reviews 62, 77–96.

Stokes, C.R., Spagnolo, M., Clark, C.D., Ó Cofaigh, C., Lian, O.B., Dunstone, R.B., 2013b. Formation of mega-scale glacial lineations on the Dubawnt Lake Ice Stream bed: 1. Size, shape and spacing from a large remote sensing dataset. Quaternary Science Reviews 77, 190–209.

Thomason, J.F., Iverson, N.R., 2006 Microfabric and micro-shear evolution in deformed till. Quaternary Science Reviews 25, 1027-1038.

Truffer, M., Harrison, W.D., Echelmeyer, K.A., 2000. Glacier motion dominated by processes deep in underlying till. Journal of Glaciology 46, 213e221. https://doi.org/10.3189/172756500781832909.

Tulaczyk, S., 1999 Ice sliding over weak, fine-grained tills: dependence of ice-till interactions on till granulometry. Special Papers Geological Society of America 337, 159-177.

Tulaczyk, S., Kamb, B., Scherer, R.P., Engelhardt, H.F., 1998. Sedimentary processes at the base of a West Antarctic ice stream: constraints from textural and compositional properties of subglacial debris. Journal of Sedimentary Research 68, 487-496.

van der Meer, J.J.M., 1987. Micromorphology of glacial sediments as a tool in distinguishing genetic varieties of till. Geological Survey of Finland Special Paper 3, 77-89.

van der Meer, J.J.M., 1993. Microscopic evidence of subglacial deformation. Quaternary Science Reviews 12, 553-587.

van der Meer, J.J.M., 1997. Particle and aggregate mobility in till: microscopic evidence of subglacial processes. Quaternary Science Reviews 16, 827-831.

van der Meer, J.J.M., Menzies, J., Rose, J., 2003. Subglacial till, the deformable glacier bed. Quaternary Science Reviews 22, 1659-1685.

van der Meer, J.J.M., Kjær, K.H., Krüger, J., Rabassa, J., Kilfeather, A.A., 2009. Under pressure: clastic dykes in glacial settings. Quaternary Science Reviews 28, 708-720.

van der Wateren, F.M., Kluiving, S.J., Bartek, L.R., 2000. Kinematic indicators of subglacial shearing. In: A.J. Maltman, B. Hubbard, M.J. Hambrey (eds.) Deformation of glacial materials. Geological Society of London, Special Publication. 176, 259-278.

Vaughan-Hirsch, D.P., Phillips, E., Lee, J.R., Hart, J.K., 2013. Micromorphological analysis of poly-phase deformation associated with the transport and emplacement of glaciotectonic rafts at West Runton, north Norfolk, UK. Boreas 42, 376–394.

Vernon, R.H., 1989. Porphyroblast-matrix microstructural relationships: recent approaches and problems. In Daly et al. (Eds), Evolution of metamorphic belts. Geological Society of London, Special Publication 43, 83-102.

# 10. Figures

**Fig. 1. (a)** and **(b)** Maps showing the location of the study area in western Poland; **(c)** Digital Elevation Model (DEM) of the Środa Wielkopolska area showing the well-developed NW-SE-trending megascale glacial lineations and locations of the trenches excavated into these subglacial landforms. Also shown is the SE-directed regional ice flow across the area; and **(d)** An example of a trench dug into the Quaternary sediments forming the landforms showing the position of the samples collected for thin sectioning. Note that the samples were collected from below the base of the soil layer.

**Fig. 2.** Microstructural map and high resolution scan of thin section C1M. The orientation of the long axes of sand to granule sized clasts included within the diamicton are shown on a series of rose diagrams. The thin section has been subdivided into 16 subareas and the E1 and E2 eigenvalues calculated for each area (see text for details).

**Fig. 3.** Microstructural map and high resolution scan of thin section C2M. The orientation of the long axes of sand to granule sized clasts included within the diamicton are shown on a series of rose diagrams. The thin section has been subdivided into 16 subareas and the E1 and E2 eigenvalues calculated for each area (see text for details).

**Fig. 4.** Microstructural map and high resolution scan of thin section C3M. The orientation of the long axes of sand to granule sized clasts included within the diamicton are shown on a series of rose

diagrams. The thin section has been subdivided into 16 subareas and the E1 and E2 eigenvalues calculated for each area (see text for details).

**Fig. 5.** Microstructural map and high resolution scan of thin section C4M. The orientation of the long axes of sand to granule sized clasts included within the diamicton are shown on a series of rose diagrams. The thin section has been subdivided into 16 subareas and the E1 and E2 eigenvalues calculated for each area (see text for details).

**Fig. 6.** Microstructural map and high resolution scan of thin section C5M. The orientation of the long axes of sand to granule sized clasts included within the diamicton are shown on a series of rose diagrams. The thin section has been subdivided into 16 subareas and the E1 and E2 eigenvalues calculated for each area (see text for details).

**Fig. 7.** Microstructural map and high resolution scan of thin section C6M. The orientation of the long axes of sand to granule sized clasts included within the diamicton are shown on a series of rose diagrams. The thin section has been subdivided into 16 subareas and the E1 and E2 eigenvalues calculated for each area (see text for details).

**Fig. 8.** Microstructural maps and automated clast density maps of the main clast microfabrics (S2, S3, S4, S5) identified within samples X1M, Y1M and Z1M.

**Fig. 9.** Photomicrographs showing the fine-grained, dusty looking carbonate which locally replaces the matrix to the diamicton (**a** to **c**) and clay lined and filled pore spaces (**d** to **f**).

**Fig. 10. (a)** Diagram showing the relationships between the different sets of Riedel shears developed within the diamicton in response to deformation imposed by the overriding ice stream; and **(b)** Example of a detailed microstructural map of sample C1M. The coloured polygons represent the different generations of clast microfabrics, which define the Riedel shears, subhorizontal shear fabric and up-ice dipping foliation.

**Fig. 11.** Graphs showing the effects of grain size on clast microfabric development within the diamicton at site C. The long axis data for each thin section (C1M to C6M) are divided into three sets: (i) grains < 0.25 mm in length; (ii) grains between 0.25 to 0.5 mm in size; and (iii) grains over > 0.5 mm in length. The number of grains in each of the three classes is plotted against the orientation of their long axis (0° represents horizontal). The large "spike" in the data set for the finest grains and total clasts at 0° results from the unavoidable "snapping" to the horizontal of short long axes dipping at very low angles (-2° to +2°) during digitisation using CorelDraw. On Figure 12 the data are plotted on a series of rose diagrams showing the dip of the long axes within the 2D plane of the thin section.

**Fig. 12.** Rose diagrams showing the variation in dip of the long axes of coarse silt to sand sized clasts within the 2D plane of the thin sections C1M to C6M. The data are divided into three sets: (i) grains < 0.25mm in length; (ii) grains between 0.25 to 0.5 mm in size; and (iii) grains over > 0.5 mm in length.

**Fig. 13.** Variation in E1 eigenvalues calculated for the thin sections (C1M to C6M) showing the variation is relative fabric strength both with an individual thin section and vertically through the diamicton at site C. Red colours represents areas of the thin sections with higher E1 values (0.65-0.68) and purple low E1 values (0.53-0.51).

**Fig. 14. (a)** Plot showing the variation in average E1 eigenvalue calculated for each thin section (C1M to C6M) with respect to depth within the diamicton sequence; and **(b)** Plot of E1 eigenvalue against shear strain. The shear strain curves for the Batestown (gravelly) and Douglas (sand-rich) tills are taken from Thomason and Iverson (2006) and are used to obtain an estimate of the range of shear strains encountered by the diamicton exposed at site C.

**Fig. 15.** Diagram showing the variation in clast microfabric development at site C.

**Fig. 16. (a)** Cartoon showing the passive rotation of elongate clasts into the plane of the developing microfabric. Further deformation of clasts aligned within this fabric is thought to occur in response to grain sliding; **(b)** Strain field diagram modified from Bell *et al*. (1986) used here to show the proposed geometry of the strain field formed in response to the presence of large immobile clasts within a weaker deforming matrix; and **(c)** Schematic diagram showing the development of anastomosing clast microfabrics within a till defined by the preferred shape alignment of finer grained clasts. The spacing of the microfabric domains is controlled by the grain size and spacing of the larger sand to pebble sized clasts in response to deformation partitioning within the till.

**Fig. 17.** Schematic profiles through the bed of a glacier and the resulting idealised cumulative strain curves: **(a)** Pervasive deformation throughout the subglacial shear zone with the amount of strain increasing upwards towards the ice-bed interface; **(b)** Deformation partitioning within the subglacial shear zone with localised detachments forming at deeper levels within the bed; and **(c)** Deformation confined to the "active" layer located at the top of the bed with shearing migrating upwards keeping pace with till accretion (cf. Larsen *et al*., 2004).

# 11. Tables

**Table 1.** Detrital clast assemblage identified within the silty sand subglacial traction till exposed at Site C.

| **Sample Number** | **Detrital Components** | |
|---|---|---|
| | ***major*** | ***minor to accessory*** |
| C1M | monocrystalline quartz, feldspar (plagioclase, K-feldspar) | polycrystalline quartz, opaque minerals, altered volcanic rocks, clinopyroxene, microcline, mudstone, sericitised granitic rock, amphibole, glauconitic material, micrographic intergrowth, ?alkali granite, garnet |
| C2M | monocrystalline quartz, feldspar (plagioclase, K-feldspar) | cryptocrystalline quartz (chert), opaque minerals, pyroxene, siltstone, mudstone, microcline, altered igneous rock, glauconitic material, micrographic intergrowth, amphibole, feldspar-chlorite rock, biotite-schistose metamorphic rock, fine sandstone (hematitic cement) |
| C3M | monocrystalline quartz | polycrystalline quartz, biotite, metamorphic rock, indurated quartz-arenite, echinoderm fragments, plagioclase, carbonate mineral(s), micritic limestone, brachiopod fragments, K-feldspar, glauconitic material, amphibole, opaque minerals, cryptocrystalline quartz (chert), very fine-grained micaceous material, epidote, siltstone/very fine-grained sandstone, foraminifera, garnet, ?zircon, muscovite |
| C4M | monocrystalline quartz, feldspar (plagioclase, K-feldspar) | micrographic intergrowth, carbonate minerals, mudstone, microcline, glauconitic material, amphibole, indurated siltstone, bioclastic limestone, glauconite-bearing micritic limestone, biotite, ?alkali granitic rock, micritic limestone, hematised siltstone, opaque minerals, altered granitic rock, ?garnet, brachiopod fragments, echinoderm fragments, quartz-epidote-rock, amphibolite |
| C5M | monocrystalline quartz | polycrystalline quartz, siltstone, amphibole, opaque minerals, carbonate minerals, micritic limestone, glauconitic material, microcline, plagioclase, altered granitic rock, devitrified igneous rock/felsite, zircon, muscovite, garnet, bioclastic limestone, glauconitic sandstone, biotite metamorphic rock |
| C6M | monocrystalline quartz | plagioclase, K-feldspar, carbonate minerals, bioclastic limestone, glauconitic material, micritic bioclastic limestone, muscovite-granite, amphibole, opaque minerals, biotite-granite, laminated siltstone, amphibolite, altered igneous rock, microcline, garnet, calcareous siltstone, very fine-grained sandstone/siltstone, zircon, epidote, tourmaline |

**Table 2.** Average E1 and E2 eigenvalues calculated for clast microfabrics developed within subglacial traction till samples C1M to C6M.

| **Depth below surface (cm)** | **Sample** | **Eigenvalues** | | | | | | | | | |
|---|---|---|---|---|---|---|---|---|---|---|---|
| | | **E1** | **E1** | **E1** | **E1** | **E1** | **E1** | **E1** | **E1** | **Median** | **Average** |
| 21 | C1M a-h | 0.555 | 0.582 | 0.578 | 0.580 | 0.582 | 0.573 | 0.570 | 0.549 | 0.575 | 0.571 |
| 24 | C1M i-p | 0.604 | 0.575 | 0.591 | 0.601 | 0.561 | 0.605 | 0.576 | 0.571 | 0.584 | 0.586 |
| 46 | C2M a-h | 0.583 | 0.588 | 0.589 | 0.631 | 0.600 | 0.565 | 0.606 | 0.562 | 0.588 | 0.590 |
| 49 | C2M i-p | 0.579 | 0.594 | 0.588 | 0.562 | 0.582 | 0.584 | 0.597 | 0.580 | 0.583 | 0.583 |
| 71 | C3M a-h | 0.649 | 0.642 | 0.618 | 0.635 | 0.654 | 0.658 | 0.651 | 0.629 | 0.646 | 0.642 |
| 74 | C3M i-p | 0.638 | 0.640 | 0.645 | 0.626 | 0.596 | 0.617 | 0.600 | 0.627 | 0.627 | 0.624 |
| 96 | C4M a-h | 0.559 | 0.540 | 0.523 | 0.550 | 0.564 | 0.561 | 0.553 | 0.586 | 0.556 | 0.555 |
| 99 | C4M i-p | 0.545 | 0.552 | 0.530 | 0.517 | 0.547 | 0.531 | 0.542 | 0.560 | 0.544 | 0.541 |
| 121 | C5M a-h | 0.521 | 0.566 | 0.541 | 0.528 | 0.557 | 0.554 | 0.557 | 0.571 | 0.555 | 0.549 |
| 124 | C5M i-p | 0.526 | 0.552 | 0.562 | 0.571 | 0.559 | 0.556 | 0.573 | 0.613 | 0.561 | 0.564 |
| 146 | C6M a-h | 0.573 | 0.556 | 0.534 | 0.571 | 0.568 | 0.551 | 0.568 | 0.582 | 0.568 | 0.563 |
| 154 | C6M i-p | 0.556 | 0.566 | 0.561 | 0.569 | 0.542 | 0.535 | 0.530 | 0.570 | 0.559 | 0.554 |
| | | **E2** | **E2** | **E2** | **E2** | **E2** | **E2** | **E2** | **E2** | **Median** | **Average** |
| 21 | C1M a-h | 0.444 | 0.417 | 0.421 | 0.419 | 0.417 | 0.426 | 0.429 | 0.450 | 0.424 | 0.428 |
| 24 | C1M i-p | 0.395 | 0.424 | 0.408 | 0.398 | 0.438 | 0.394 | 0.423 | 0.428 | 0.415 | 0.413 |
| 46 | C2M a-h | 0.416 | 0.411 | 0.410 | 0.368 | 0.399 | 0.434 | 0.393 | 0.437 | 0.411 | 0.409 |
| 49 | C2M i-p | 0.420 | 0.405 | 0.411 | 0.437 | 0.417 | 0.415 | 0.402 | 0.419 | 0.416 | 0.416 |

| | | | | | | | | | | | |
|---|---|---|---|---|---|---|---|---|---|---|---|
| 71 | C3M a-h | 0.350 | 0.357 | 0.381 | 0.364 | 0.345 | 0.341 | 0.348 | 0.370 | 0.353 | 0.357 |
| 74 | C3M i-p | 0.361 | 0.359 | 0.354 | 0.373 | 0.403 | 0.382 | 0.399 | 0.372 | 0.372 | 0.375 |
| 96 | C4M a-h | 0.440 | 0.459 | 0.476 | 0.449 | 0.435 | 0.438 | 0.446 | 0.413 | 0.443 | 0.444 |
| 99 | C4M i-p | 0.454 | 0.447 | 0.469 | 0.482 | 0.452 | 0.468 | 0.457 | 0.439 | 0.455 | 0.458 |
| 121 | C5M a-h | 0.478 | 0.43 | 0.458 | 0.471 | 0.442 | 0.445 | 0.442 | 0.428 | 0.444 | 0.450 |
| 124 | C5M i-p | 0.473 | 0.447 | 0.437 | 0.428 | 0.440 | 0.443 | 0.426 | 0.386 | 0.438 | 0.435 |
| 146 | C6M a-h | 0.426 | 0.443 | 0.465 | 0.428 | 0.431 | 0.448 | 0.431 | 0.417 | 0.431 | 0.436 |
| 154 | C6M a-p | 0.443 | 0.433 | 0.438 | 0.430 | 0.457 | 0.464 | 0.469 | 0.429 | 0.440 | 0.445 |

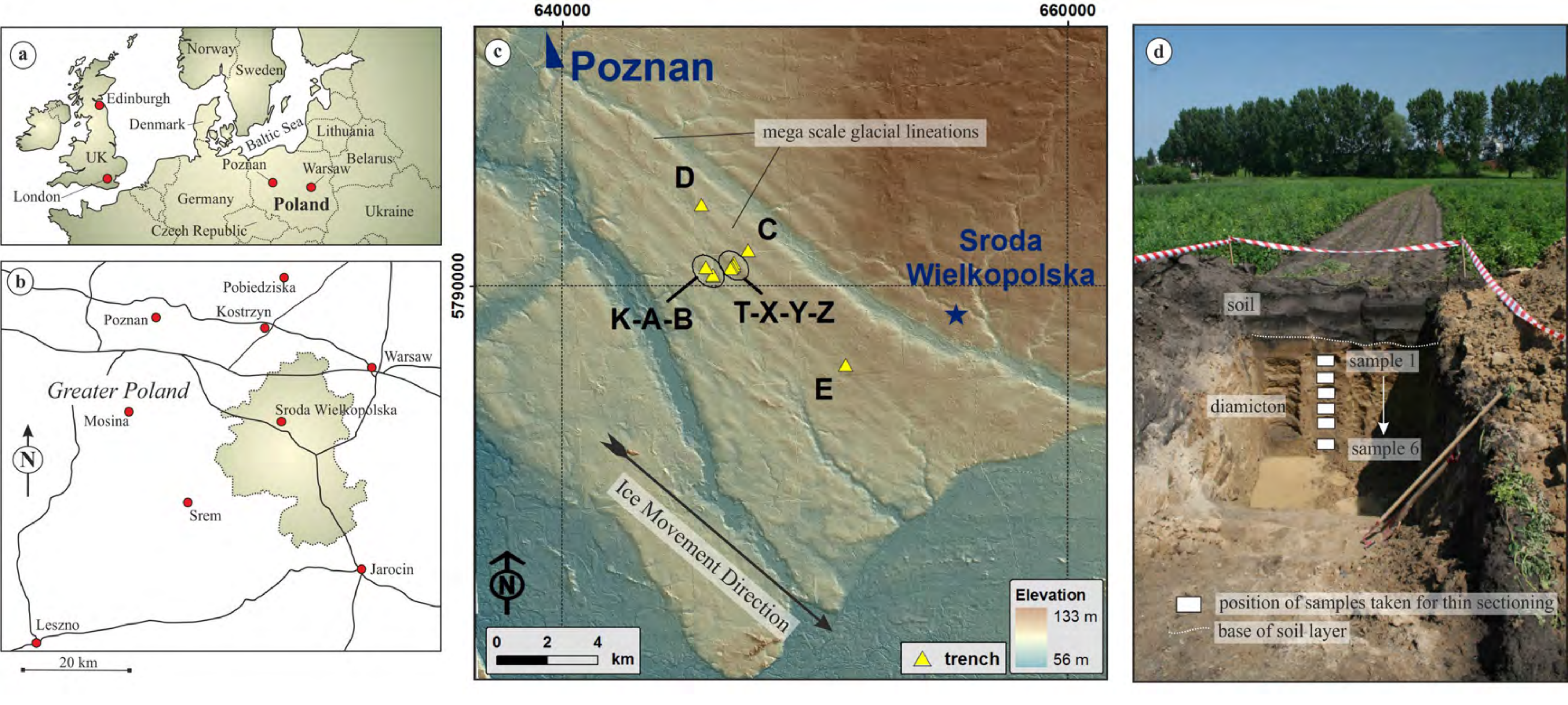

a
Norway
Sweden
Edinburgh
Denmark
Baltic Sea
Lithuania
UK
Poznan
Warsaw
Belarus
London
Germany
Poland
Ukraine
Czech Republic
b
Pobiedziska
Poznan
Kostrzyn
Warsaw
Greater Poland
Sroda Wielkopolska
Mosina
N
Srem
Jarocin
Leszno
20 km
c
640000
660000
5790000
Poznan
mega scale glacial lineations
D
C
Sroda
Wielkopolska
K-A-B
T-X-Y-Z
E
Ice Movement Direction
N
0 2 4 km
trench
Elevation
133 m
56 m
d
soil
sample 1
diamicton
sample 6
position of samples taken for thin sectioning
base of soil layer

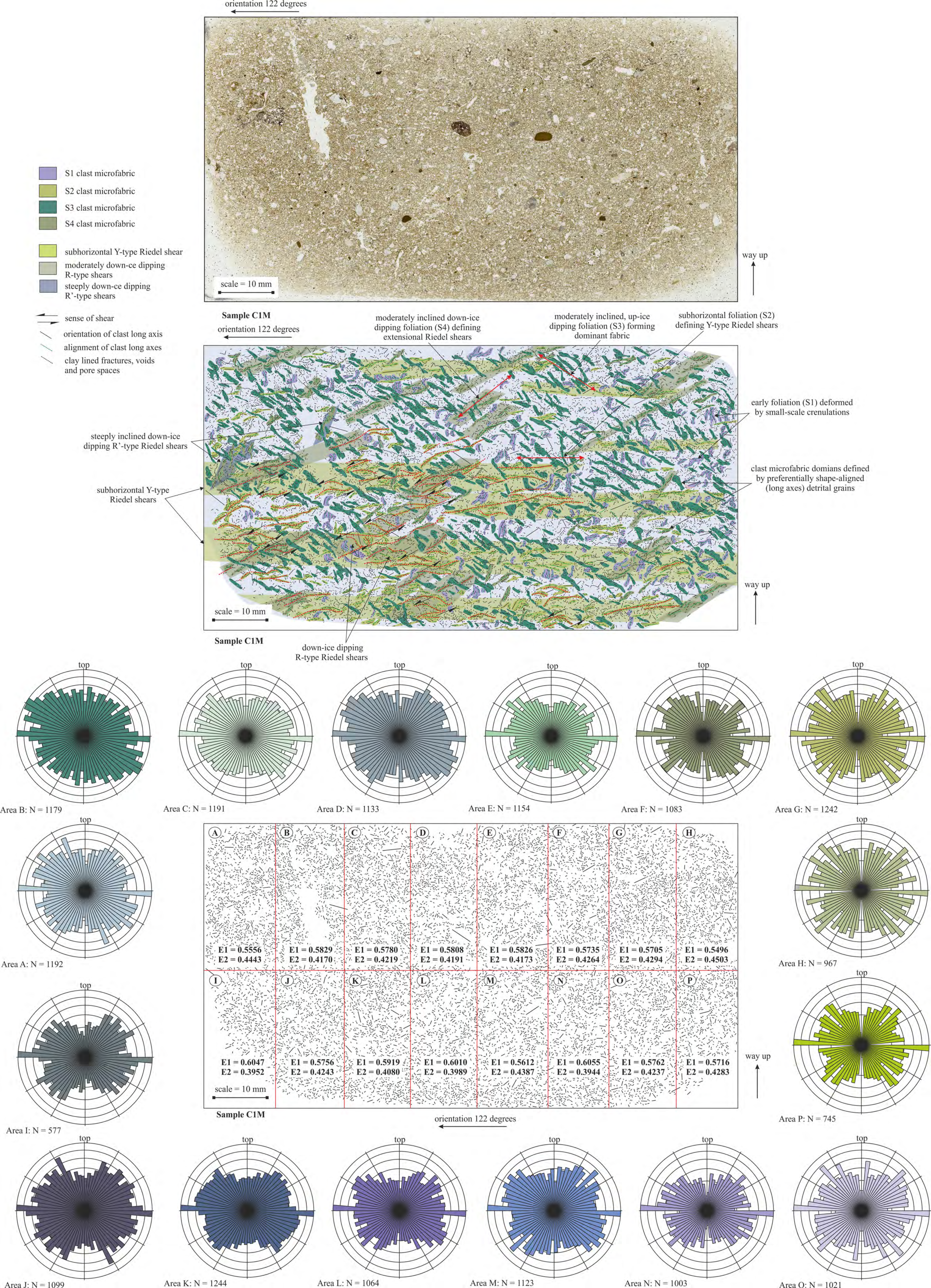

orientation 122 degrees
scale = 10 mm
way up
Sample C1M
S1 clast microfabric
S2 clast microfabric
S3 clast microfabric
S4 clast microfabric
subhorizontal Y-type Riedel shear
moderately down-ce dipping R-type shears
steeply down-ce dipping R'-type shears
sense of shear
orientation of clast long axis
alignment of clast long axes
clay lined fractures, voids and pore spaces
orientation 122 degrees
moderately inclined down-ice dipping foliation (S4) defining extensional Riedel shears
moderately inclined, up-ice dipping foliation (S3) forming dominant fabric
subhorizontal foliation (S2) defining Y-type Riedel shears
early foliation (S1) deformed by small-scale crenulations
steeply inclined down-ice dipping R'-type Riedel shears
clast microfabric domians defined by preferentially shape-aligned (long axes) detrital grains
subhorizontal Y-type Riedel shears
way up
scale = 10 mm
Sample C1M
down-ice dipping R-type Riedel shears
top
Area B: N = 1179
Area C: N = 1191
Area D: N = 1133
Area E: N = 1154
Area F: N = 1083
Area G: N = 1242
Area A: N = 1192
A
E1 = 0.5556
E2 = 0.4443
B
E1 = 0.5829
E2 = 0.4170
C
E1 = 0.5780
E2 = 0.4219
D
E1 = 0.5808
E2 = 0.4191
E
E1 = 0.5826
E2 = 0.4173
F
E1 = 0.5735
E2 = 0.4264
G
E1 = 0.5705
E2 = 0.4294
H
E1 = 0.5496
E2 = 0.4503
Area H: N = 967
I
E1 = 0.6047
E2 = 0.3952
J
E1 = 0.5756
E2 = 0.4243
K
E1 = 0.5919
E2 = 0.4080
L
E1 = 0.6010
E2 = 0.3989
M
E1 = 0.5612
E2 = 0.4387
N
E1 = 0.6055
E2 = 0.3944
O
E1 = 0.5762
E2 = 0.4237
P
E1 = 0.5716
E2 = 0.4283
scale = 10 mm
Sample C1M
orientation 122 degrees
way up
Area I: N = 577
Area P: N = 745
Area J: N = 1099
Area K: N = 1244
Area L: N = 1064
Area M: N = 1123
Area N: N = 1003
Area O: N = 1021

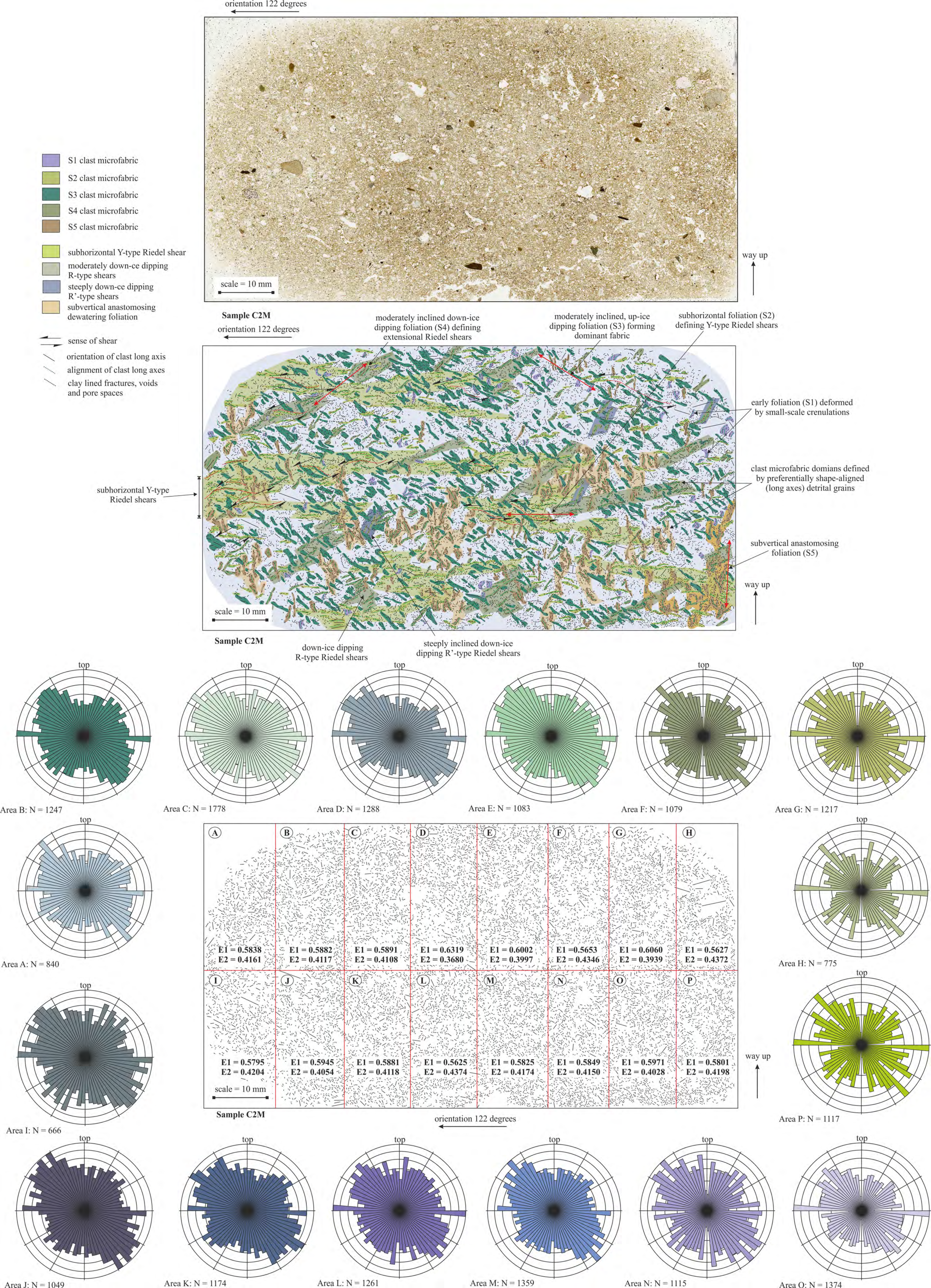

orientation 122 degrees
way up
scale = 10 mm
S1 clast microfabric
S2 clast microfabric
S3 clast microfabric
S4 clast microfabric
S5 clast microfabric
subhorizontal Y-type Riedel shear
moderately down-ce dipping R-type shears
steeply down-ce dipping R'-type shears
subvertical anastomosing dewatering foliation
sense of shear
orientation of clast long axis
alignment of clast long axes
clay lined fractures, voids and pore spaces
Sample C2M
orientation 122 degrees
moderately inclined down-ice dipping foliation (S4) defining extensional Riedel shears
moderately inclined, up-ice dipping foliation (S3) forming dominant fabric
subhorizontal foliation (S2) defining Y-type Riedel shears
early foliation (S1) deformed by small-scale crenulations
clast microfabric domians defined by preferentially shape-aligned (long axes) detrital grains
subhorizontal Y-type Riedel shears
subvertical anastomosing foliation (S5)
way up
scale = 10 mm
Sample C2M
down-ice dipping R-type Riedel shears
steeply inclined down-ice dipping R'-type Riedel shears
top
Area B: N = 1247
Area C: N = 1778
Area D: N = 1288
Area E: N = 1083
Area F: N = 1079
Area G: N = 1217
Area A: N = 840
Area H: N = 775
A B C D E F G H
E1 = 0.5838 E2 = 0.4161
E1 = 0.5882 E2 = 0.4117
E1 = 0.5891 E2 = 0.4108
E1 = 0.6319 E2 = 0.3680
E1 = 0.6002 E2 = 0.3997
E1 = 0.5653 E2 = 0.4346
E1 = 0.6060 E2 = 0.3939
E1 = 0.5627 E2 = 0.4372
I J K L M N O P
E1 = 0.5795 E2 = 0.4204
E1 = 0.5945 E2 = 0.4054
E1 = 0.5881 E2 = 0.4118
E1 = 0.5625 E2 = 0.4374
E1 = 0.5825 E2 = 0.4174
E1 = 0.5849 E2 = 0.4150
E1 = 0.5971 E2 = 0.4028
E1 = 0.5801 E2 = 0.4198
scale = 10 mm
way up
Sample C2M
orientation 122 degrees
Area I: N = 666
Area P: N = 1117
Area J: N = 1049
Area K: N = 1174
Area L: N = 1261
Area M: N = 1359
Area N: N = 1115
Area O: N = 1374

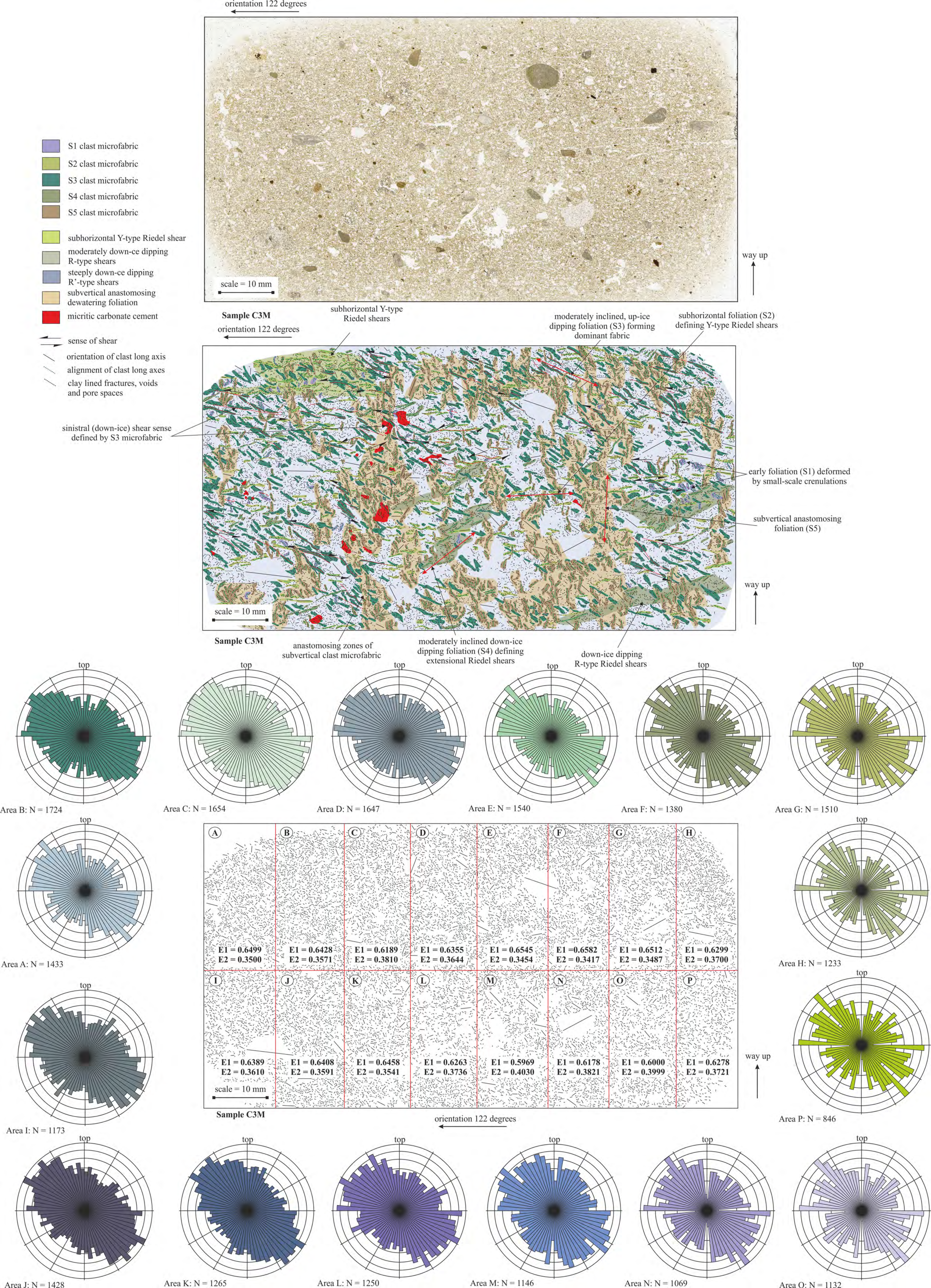

orientation 122 degrees
scale = 10 mm
way up
Sample C3M
S1 clast microfabric
S2 clast microfabric
S3 clast microfabric
S4 clast microfabric
S5 clast microfabric
subhorizontal Y-type Riedel shear
moderately down-ce dipping R-type shears
steeply down-ce dipping R'-type shears
subvertical anastomosing dewatering foliation
micritic carbonate cement
sense of shear
orientation of clast long axis
alignment of clast long axes
clay lined fractures, voids and pore spaces
subhorizontal Y-type Riedel shears
orientation 122 degrees
moderately inclined, up-ice dipping foliation (S3) forming dominant fabric
subhorizontal foliation (S2) defining Y-type Riedel shears
sinistral (down-ice) shear sense defined by S3 microfabric
early foliation (S1) deformed by small-scale crenulations
subvertical anastomosing foliation (S5)
way up
scale = 10 mm
Sample C3M
anastomosing zones of subvertical clast microfabric
moderately inclined down-ice dipping foliation (S4) defining extensional Riedel shears
down-ice dipping R-type Riedel shears
top
Area B: N = 1724
Area C: N = 1654
Area D: N = 1647
Area E: N = 1540
Area F: N = 1380
Area G: N = 1510
Area A: N = 1433
Area H: N = 1233
A
B
C
D
E
F
G
H
E1 = 0.6499
E2 = 0.3500
E1 = 0.6428
E2 = 0.3571
E1 = 0.6189
E2 = 0.3810
E1 = 0.6355
E2 = 0.3644
E1 = 0.6545
E2 = 0.3454
E1 = 0.6582
E2 = 0.3417
E1 = 0.6512
E2 = 0.3487
E1 = 0.6299
E2 = 0.3700
I
J
K
L
M
N
O
P
E1 = 0.6389
E2 = 0.3610
E1 = 0.6408
E2 = 0.3591
E1 = 0.6458
E2 = 0.3541
E1 = 0.6263
E2 = 0.3736
E1 = 0.5969
E2 = 0.4030
E1 = 0.6178
E2 = 0.3821
E1 = 0.6000
E2 = 0.3999
E1 = 0.6278
E2 = 0.3721
scale = 10 mm
Sample C3M
way up
orientation 122 degrees
Area I: N = 1173
Area P: N = 846
Area J: N = 1428
Area K: N = 1265
Area L: N = 1250
Area M: N = 1146
Area N: N = 1069
Area O: N = 1132

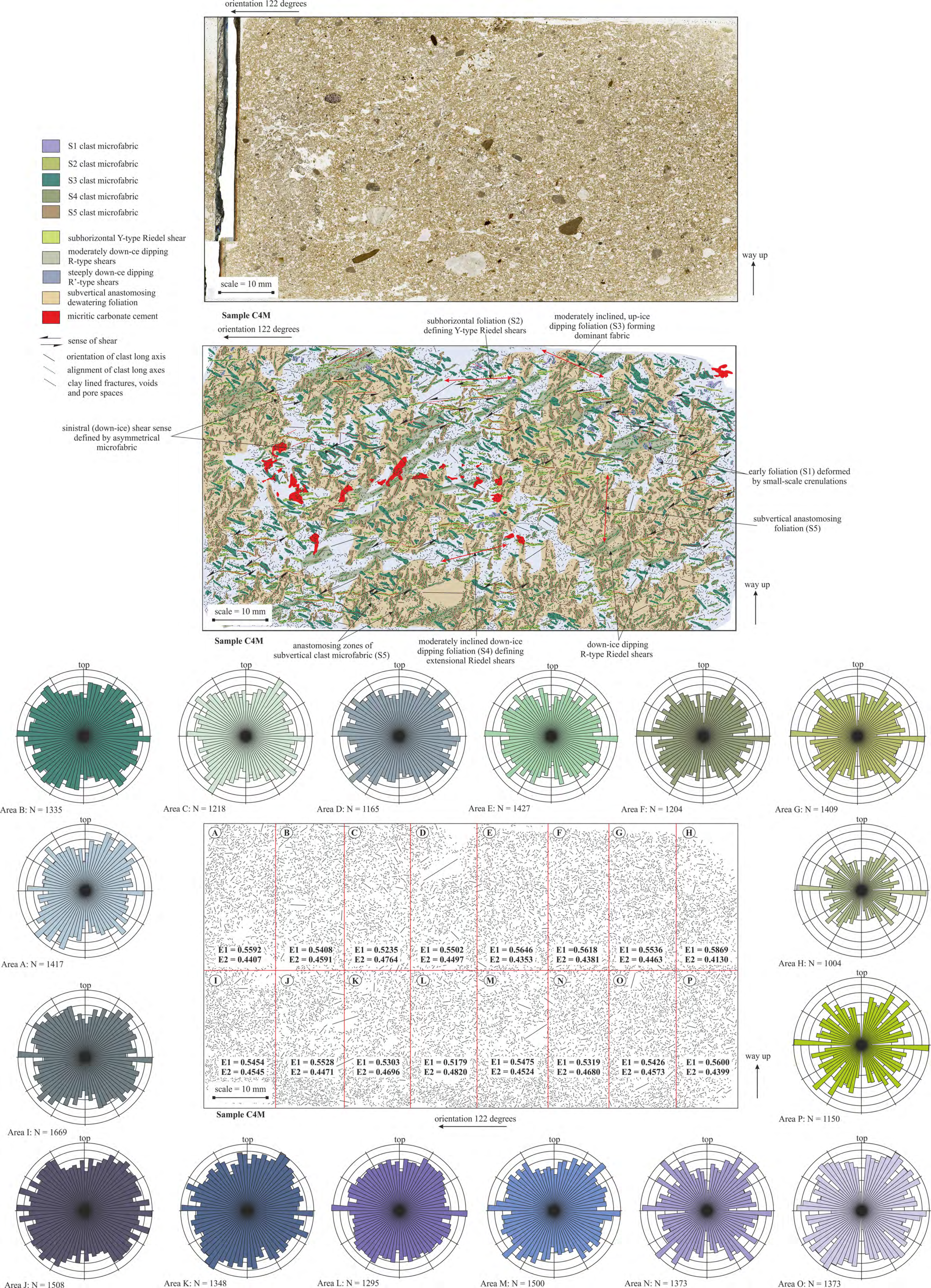
orientation 122 degrees
S1 clast microfabric
S2 clast microfabric
S3 clast microfabric
S4 clast microfabric
S5 clast microfabric
subhorizontal Y-type Riedel shear
moderately down-ce dipping R-type shears
steeply down-ce dipping R'-type shears
subvertical anastomosing dewatering foliation
micritic carbonate cement
sense of shear
orientation of clast long axis
alignment of clast long axes
clay lined fractures, voids and pore spaces
scale = 10 mm
way up
Sample C4M
orientation 122 degrees
subhorizontal foliation (S2) defining Y-type Riedel shears
moderately inclined, up-ice dipping foliation (S3) forming dominant fabric
sinistral (down-ice) shear sense defined by asymmetrical microfabric
early foliation (S1) deformed by small-scale crenulations
subvertical anastomosing foliation (S5)
way up
scale = 10 mm
Sample C4M
anastomosing zones of subvertical clast microfabric (S5)
moderately inclined down-ice dipping foliation (S4) defining extensional Riedel shears
down-ice dipping R-type Riedel shears
top
Area B: N = 1335
Area C: N = 1218
Area D: N = 1165
Area E: N = 1427
Area F: N = 1204
Area G: N = 1409
Area A: N = 1417
Area H: N = 1004
A B C D E F G H
E1 = 0.5592 E2 = 0.4407
E1 = 0.5408 E2 = 0.4591
E1 = 0.5235 E2 = 0.4764
E1 = 0.5502 E2 = 0.4497
E1 = 0.5646 E2 = 0.4353
E1 = 0.5618 E2 = 0.4381
E1 = 0.5536 E2 = 0.4463
E1 = 0.5869 E2 = 0.4130
I J K L M N O P
E1 = 0.5454 E2 = 0.4545
E1 = 0.5528 E2 = 0.4471
E1 = 0.5303 E2 = 0.4696
E1 = 0.5179 E2 = 0.4820
E1 = 0.5475 E2 = 0.4524
E1 = 0.5319 E2 = 0.4680
E1 = 0.5426 E2 = 0.4573
E1 = 0.5600 E2 = 0.4399
scale = 10 mm
way up
Sample C4M
orientation 122 degrees
Area I: N = 1669
Area P: N = 1150
Area J: N = 1508
Area K: N = 1348
Area L: N = 1295
Area M: N = 1500
Area N: N = 1373
Area O: N = 1373

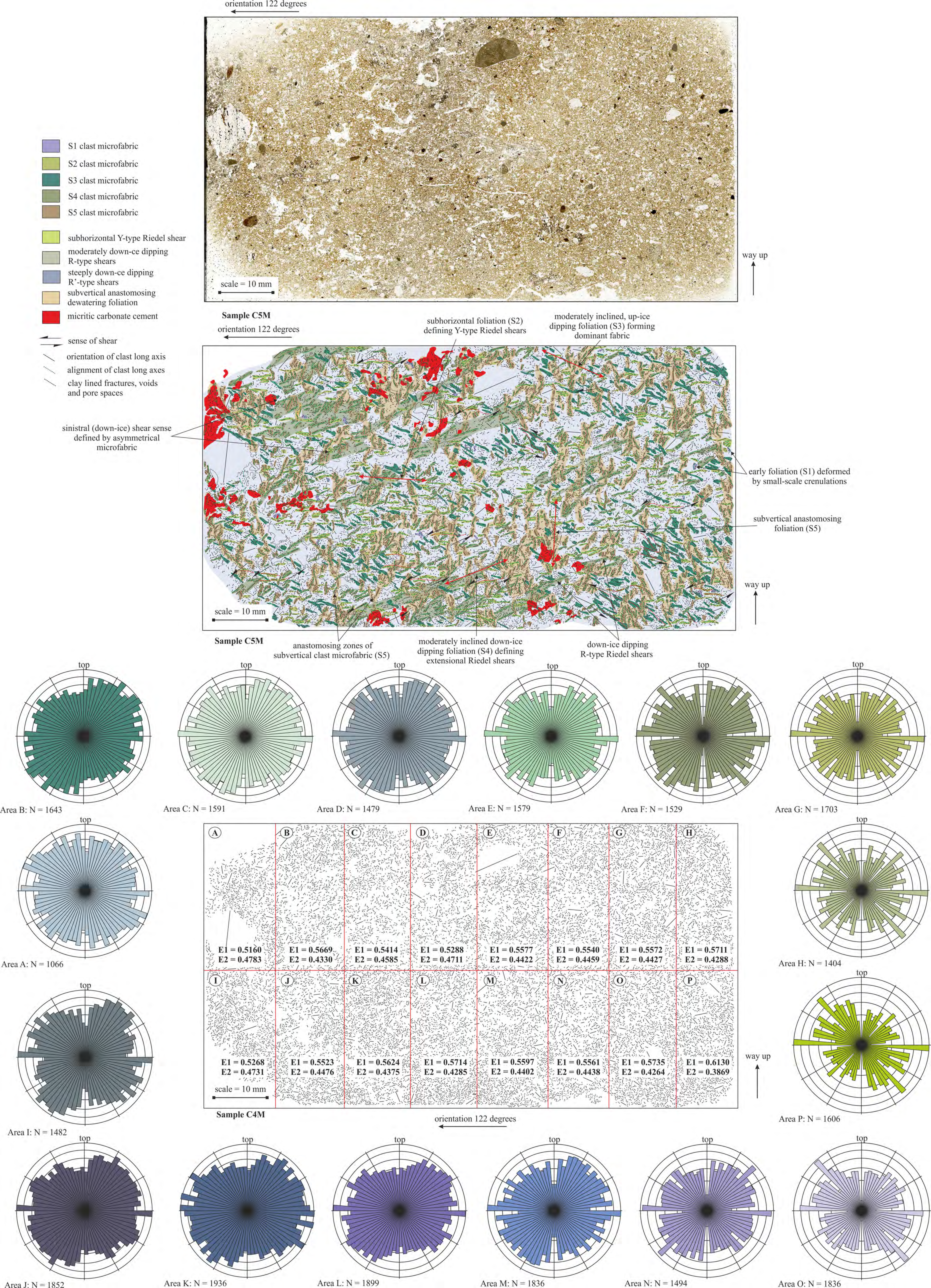

orientation 122 degrees
scale = 10 mm
way up
Sample C5M
S1 clast microfabric
S2 clast microfabric
S3 clast microfabric
S4 clast microfabric
S5 clast microfabric
subhorizontal Y-type Riedel shear
moderately down-ce dipping R-type shears
steeply down-ce dipping R'-type shears
subvertical anastomosing dewatering foliation
micritic carbonate cement
sense of shear
orientation of clast long axis
alignment of clast long axes
clay lined fractures, voids and pore spaces
orientation 122 degrees
subhorizontal foliation (S2) defining Y-type Riedel shears
moderately inclined, up-ice dipping foliation (S3) forming dominant fabric
sinistral (down-ice) shear sense defined by asymmetrical microfabric
early foliation (S1) deformed by small-scale crenulations
subvertical anastomosing foliation (S5)
way up
scale = 10 mm
Sample C5M
anastomosing zones of subvertical clast microfabric (S5)
moderately inclined down-ice dipping foliation (S4) defining extensional Riedel shears
down-ice dipping R-type Riedel shears
top
Area B: N = 1643
Area C: N = 1591
Area D: N = 1479
Area E: N = 1579
Area F: N = 1529
Area G: N = 1703
Area A: N = 1066
Area H: N = 1404
A
B
C
D
E
F
G
H
E1 = 0.5160
E2 = 0.4783
E1 = 0.5669
E2 = 0.4330
E1 = 0.5414
E2 = 0.4585
E1 = 0.5288
E2 = 0.4711
E1 = 0.5577
E2 = 0.4422
E1 = 0.5540
E2 = 0.4459
E1 = 0.5572
E2 = 0.4427
E1 = 0.5711
E2 = 0.4288
I
J
K
L
M
N
O
P
E1 = 0.5268
E2 = 0.4731
E1 = 0.5523
E2 = 0.4476
E1 = 0.5624
E2 = 0.4375
E1 = 0.5714
E2 = 0.4285
E1 = 0.5597
E2 = 0.4402
E1 = 0.5561
E2 = 0.4438
E1 = 0.5735
E2 = 0.4264
E1 = 0.6130
E2 = 0.3869
scale = 10 mm
way up
Sample C4M
orientation 122 degrees
Area I: N = 1482
Area P: N = 1606
Area J: N = 1852
Area K: N = 1936
Area L: N = 1899
Area M: N = 1836
Area N: N = 1494
Area O: N = 1836

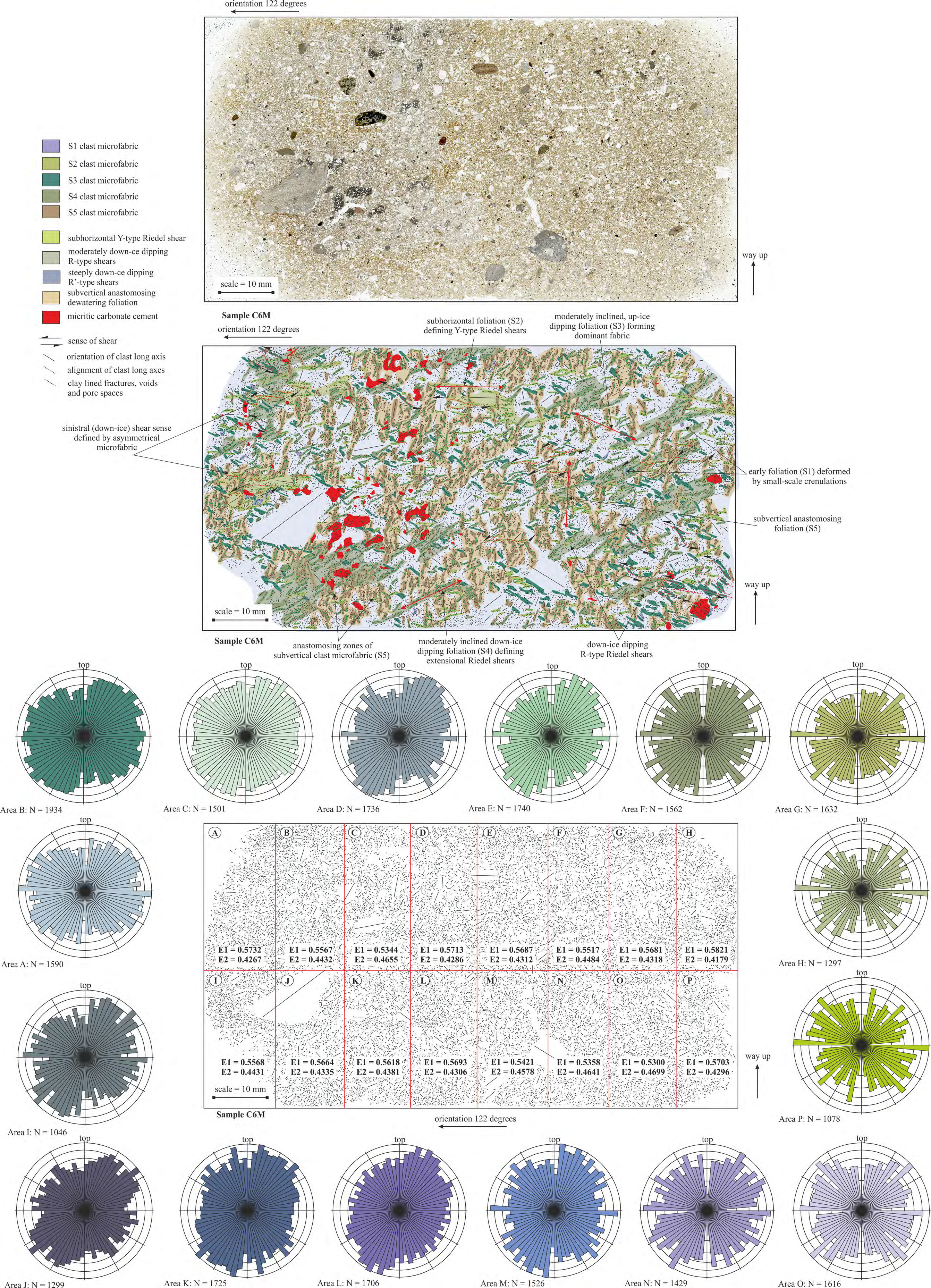
orientation 122 degrees
scale = 10 mm
way up
S1 clast microfabric
S2 clast microfabric
S3 clast microfabric
S4 clast microfabric
S5 clast microfabric
subhorizontal Y-type Riedel shear
moderately down-ce dipping R-type shears
steeply down-ce dipping R'-type shears
subvertical anastomosing dewatering foliation
micritic carbonate cement
sense of shear
orientation of clast long axis
alignment of clast long axes
clay lined fractures, voids and pore spaces
Sample C6M
orientation 122 degrees
subhorizontal foliation (S2) defining Y-type Riedel shears
moderately inclined, up-ice dipping foliation (S3) forming dominant fabric
sinistral (down-ice) shear sense defined by asymmetrical microfabric
early foliation (S1) deformed by small-scale crenulations
subvertical anastomosing foliation (S5)
way up
scale = 10 mm
Sample C6M
anastomosing zones of subvertical clast microfabric (S5)
moderately inclined down-ice dipping foliation (S4) defining extensional Riedel shears
down-ice dipping R-type Riedel shears
top
Area B: N = 1934
Area C: N = 1501
Area D: N = 1736
Area E: N = 1740
Area F: N = 1562
Area G: N = 1632
Area A: N = 1590
Area H: N = 1297
A
B
C
D
E
F
G
H
E1 = 0.5732
E2 = 0.4267
E1 = 0.5567
E2 = 0.4432
E1 = 0.5344
E2 = 0.4655
E1 = 0.5713
E2 = 0.4286
E1 = 0.5687
E2 = 0.4312
E1 = 0.5517
E2 = 0.4484
E1 = 0.5681
E2 = 0.4318
E1 = 0.5821
E2 = 0.4179
I
J
K
L
M
N
O
P
E1 = 0.5568
E2 = 0.4431
E1 = 0.5664
E2 = 0.4335
E1 = 0.5618
E2 = 0.4381
E1 = 0.5693
E2 = 0.4306
E1 = 0.5421
E2 = 0.4578
E1 = 0.5358
E2 = 0.4641
E1 = 0.5300
E2 = 0.4699
E1 = 0.5703
E2 = 0.4296
scale = 10 mm
way up
Sample C6M
orientation 122 degrees
Area I: N = 1046
Area P: N = 1078
Area J: N = 1299
Area K: N = 1725
Area L: N = 1706
Area M: N = 1526
Area N: N = 1429
Area O: N = 1616

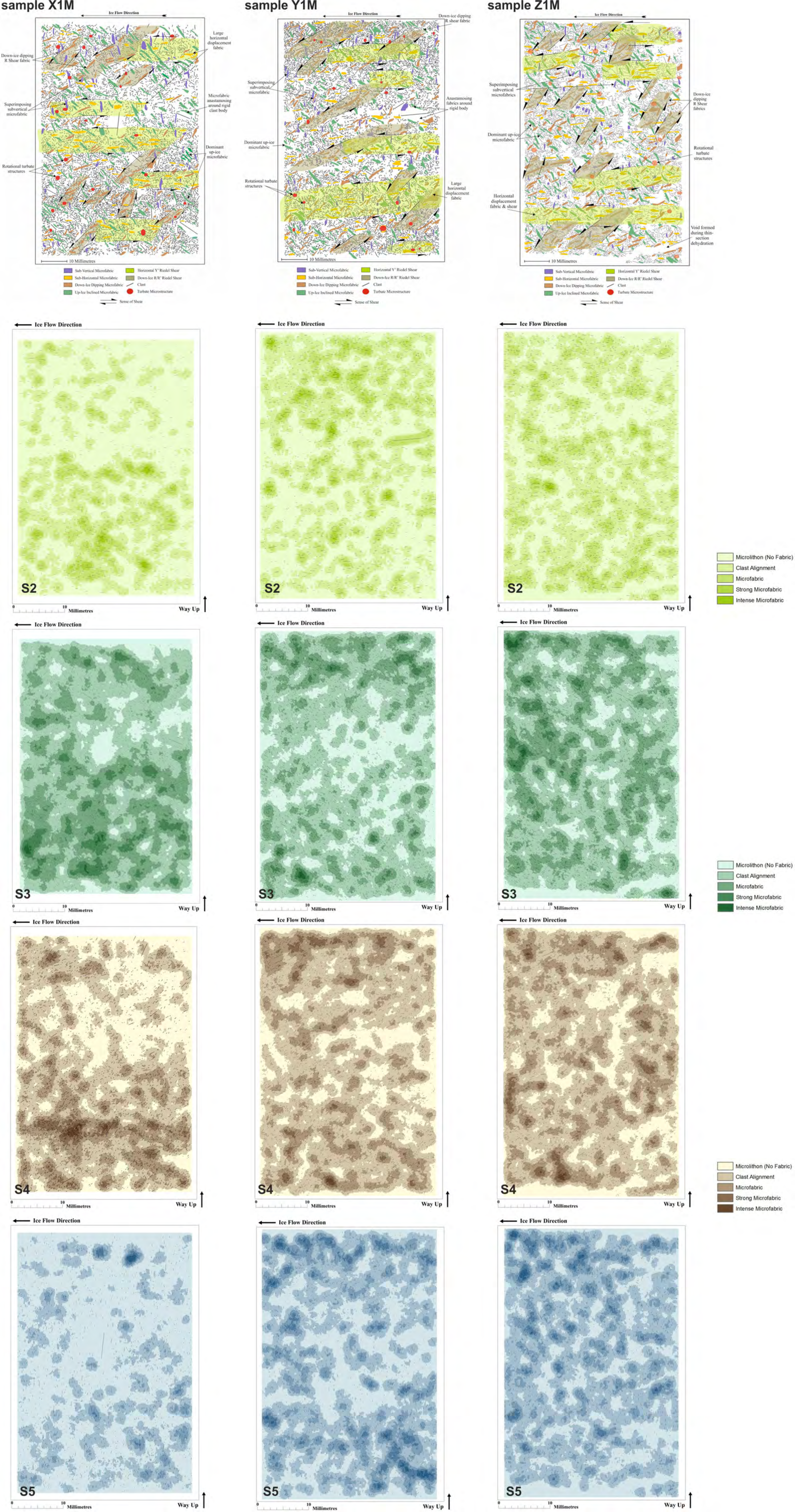

sample X1M
sample Y1M
sample Z1M
Ice Flow Direction
Down-ice dipping R Shear fabric
Large horizontal displacement fabric
Superimposing subvertical microfabric
Microfabric anastamosing around rigid clast body
Dominant up-ice microfabric
Rotational turbate structures
Anastamosing fabrics around rigid body
Horizontal displacement fabric & shear
Void formed during thin-section dehydration
10 Millimetres
Sub-Vertical Microfabric
Sub-Horizontal Microfabric
Down-Ice Dipping Microfabric
Up-Ice Inclined Microfabric
Horizontal 'Y' Riedel Shear
Down-Ice R/R' Riedel Shear
Clast
Turbate Microstructure
Sense of Shear
S2
S3
S4
S5
Millimetres
Way Up
Microlithon (No Fabric)
Clast Alignment
Microfabric
Strong Microfabric
Intense Microfabric

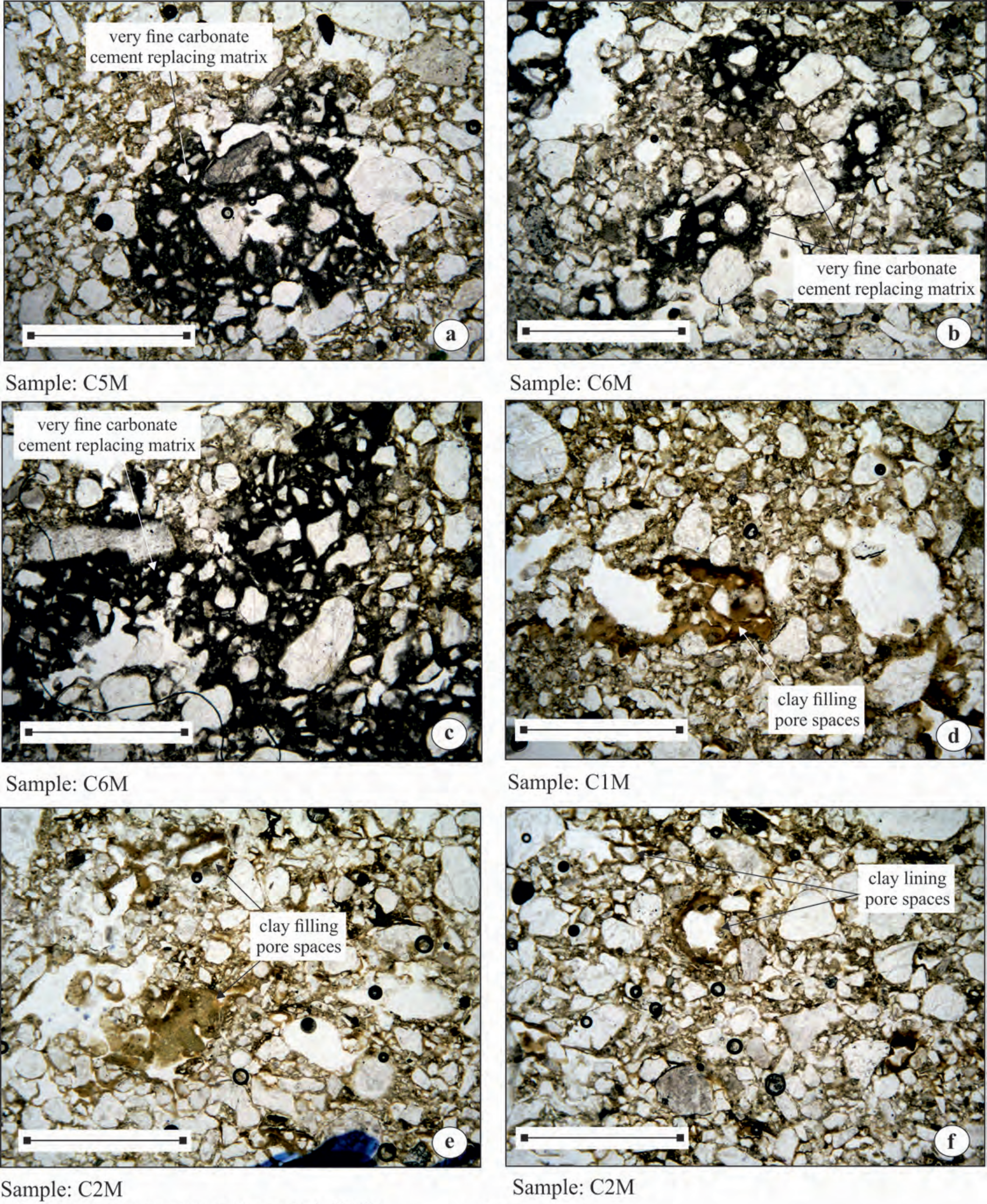


all photomicrographs taken in plane polarised light

scale bar = 1 mm

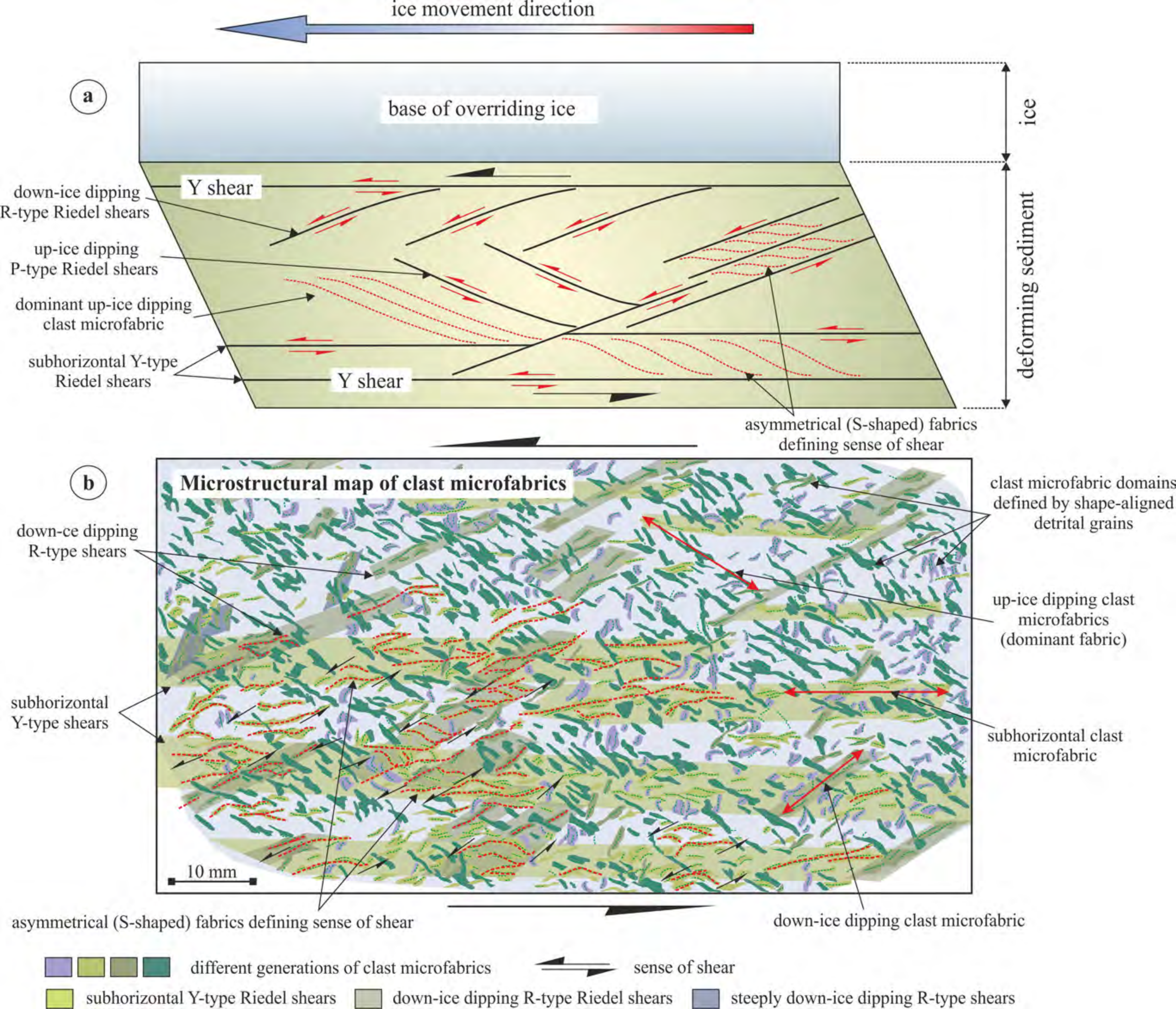
ice movement direction
a
base of overriding ice
ice
deforming sediment
Y shear
down-ice dipping
R-type Riedel shears
up-ice dipping
P-type Riedel shears
dominant up-ice dipping
clast microfabric
subhorizontal Y-type
Riedel shears
Y shear
asymmetrical (S-shaped) fabrics
defining sense of shear
b
Microstructural map of clast microfabrics
down-ce dipping
R-type shears
subhorizontal
Y-type shears
clast microfabric domains
defined by shape-aligned
detrital grains
up-ice dipping clast
microfabrics
(dominant fabric)
subhorizontal clast
microfabric
10 mm
asymmetrical (S-shaped) fabrics defining sense of shear
down-ice dipping clast microfabric
different generations of clast microfabrics
sense of shear
subhorizontal Y-type Riedel shears
down-ice dipping R-type Riedel shears
steeply down-ice dipping R-type shears

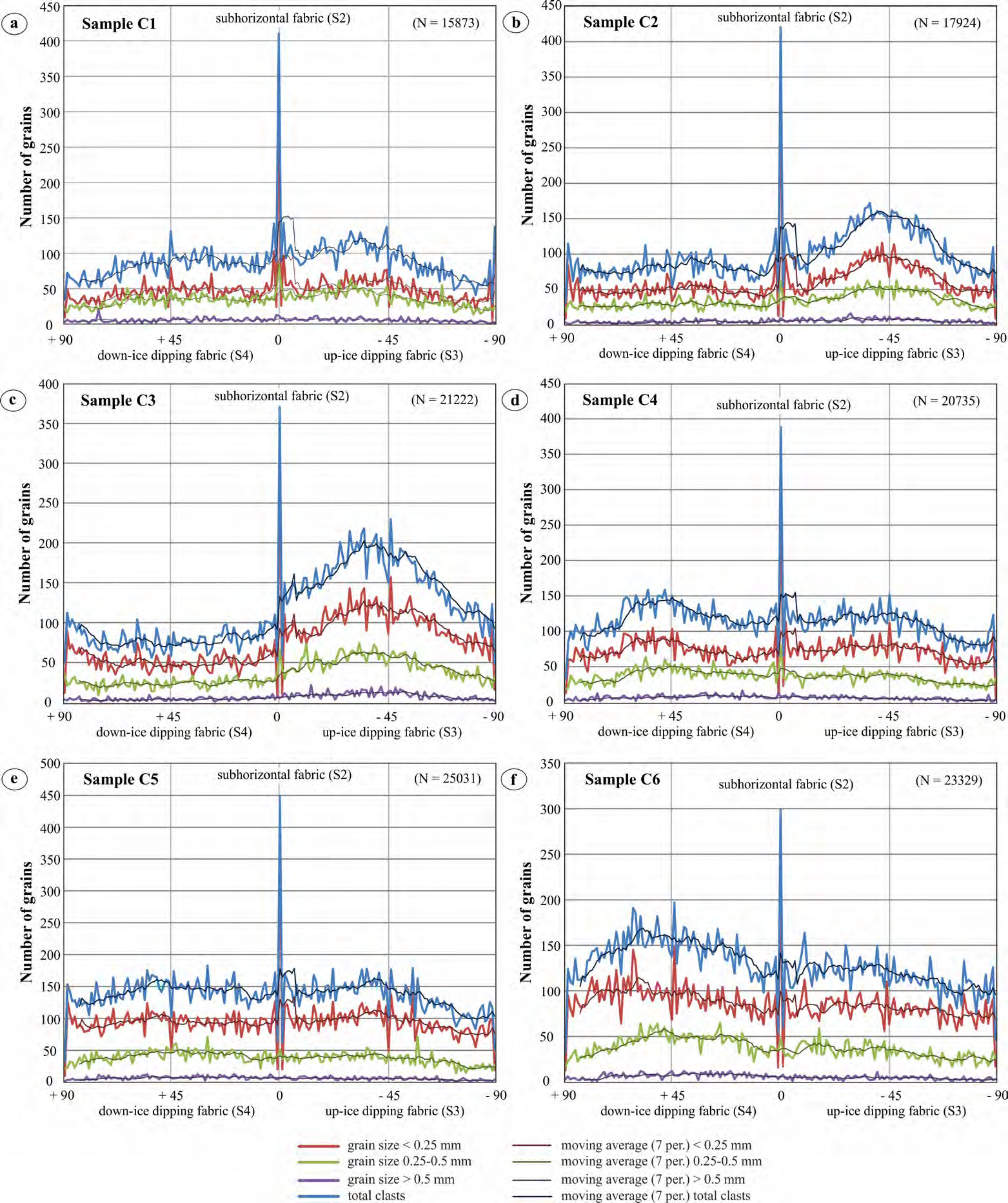
a
Sample C1
subhorizontal fabric (S2)
(N = 15873)
b
Sample C2
subhorizontal fabric (S2)
(N = 17924)
c
Sample C3
subhorizontal fabric (S2)
(N = 21222)
d
Sample C4
subhorizontal fabric (S2)
(N = 20735)
e
Sample C5
subhorizontal fabric (S2)
(N = 25031)
f
Sample C6
subhorizontal fabric (S2)
(N = 23329)
Number of grains
+ 90
+ 45
0
- 45
- 90
down-ice dipping fabric (S4)
up-ice dipping fabric (S3)
grain size < 0.25 mm
grain size 0.25-0.5 mm
grain size > 0.5 mm
total clasts
moving average (7 per.) < 0.25 mm
moving average (7 per.) 0.25-0.5 mm
moving average (7 per.) > 0.5 mm
moving average (7 per.) total clasts

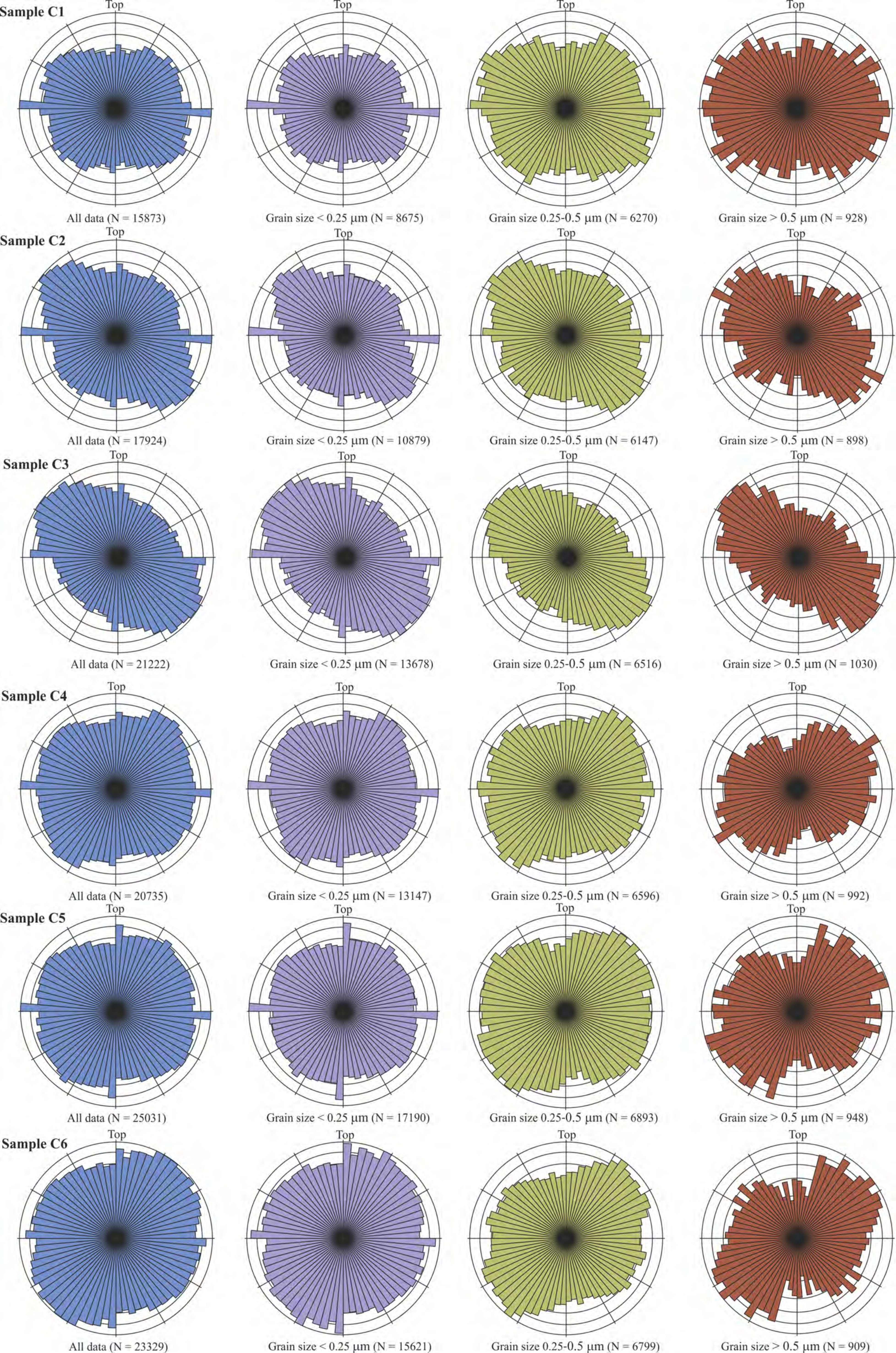
Sample C1
Top
Top
Top
Top
All data (N = 15873)
Grain size < 0.25 μm (N = 8675)
Grain size 0.25-0.5 μm (N = 6270)
Grain size > 0.5 μm (N = 928)
Sample C2
Top
Top
Top
Top
All data (N = 17924)
Grain size < 0.25 μm (N = 10879)
Grain size 0.25-0.5 μm (N = 6147)
Grain size > 0.5 μm (N = 898)
Sample C3
Top
Top
Top
Top
All data (N = 21222)
Grain size < 0.25 μm (N = 13678)
Grain size 0.25-0.5 μm (N = 6516)
Grain size > 0.5 μm (N = 1030)
Sample C4
Top
Top
Top
Top
All data (N = 20735)
Grain size < 0.25 μm (N = 13147)
Grain size 0.25-0.5 μm (N = 6596)
Grain size > 0.5 μm (N = 992)
Sample C5
Top
Top
Top
Top
All data (N = 25031)
Grain size < 0.25 μm (N = 17190)
Grain size 0.25-0.5 μm (N = 6893)
Grain size > 0.5 μm (N = 948)
Sample C6
Top
Top
Top
Top
All data (N = 23329)
Grain size < 0.25 μm (N = 15621)
Grain size 0.25-0.5 μm (N = 6799)
Grain size > 0.5 μm (N = 909)


orientation 122 degrees
ranges in E1 values
0.680
0.670
0.660
0.650
0.640
0.630
0.620
0.610
0.600
0.590
0.580
0.570
0.560
0.550
0.540
0.530
0.520
0.510
way up
scale = 10 mm
Sample C1M
way up
scale = 10 mm
Sample C2M
way up
scale = 10 mm
Sample C3M
way up
scale = 10 mm
Sample C4M
way up
scale = 10 mm
Sample C5M
way up
scale = 10 mm
Sample C6M

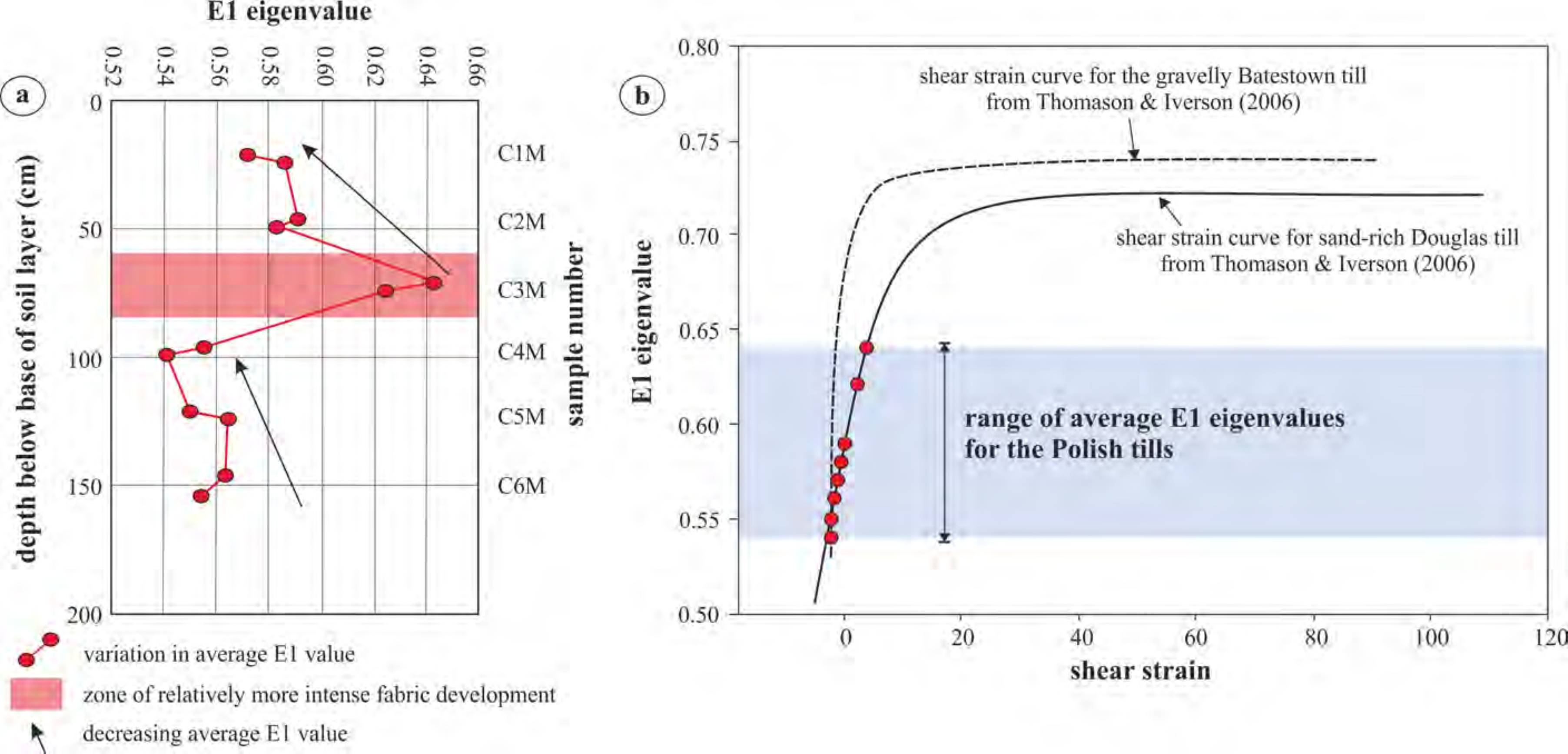

E1 eigenvalue
0.52
0.54
0.56
0.58
0.60
0.62
0.64
0.66
a
0
50
100
150
200
depth below base of soil layer (cm)
C1M
C2M
C3M
C4M
C5M
C6M
sample number
variation in average E1 value
zone of relatively more intense fabric development
decreasing average E1 value
b
0.80
0.75
0.70
0.65
0.60
0.55
0.50
E1 eigenvalue
shear strain curve for the gravelly Batestown till
from Thomason & Iverson (2006)
shear strain curve for sand-rich Douglas till
from Thomason & Iverson (2006)
range of average E1 eigenvalues
for the Polish tills
0
20
40
60
80
100
120
shear strain

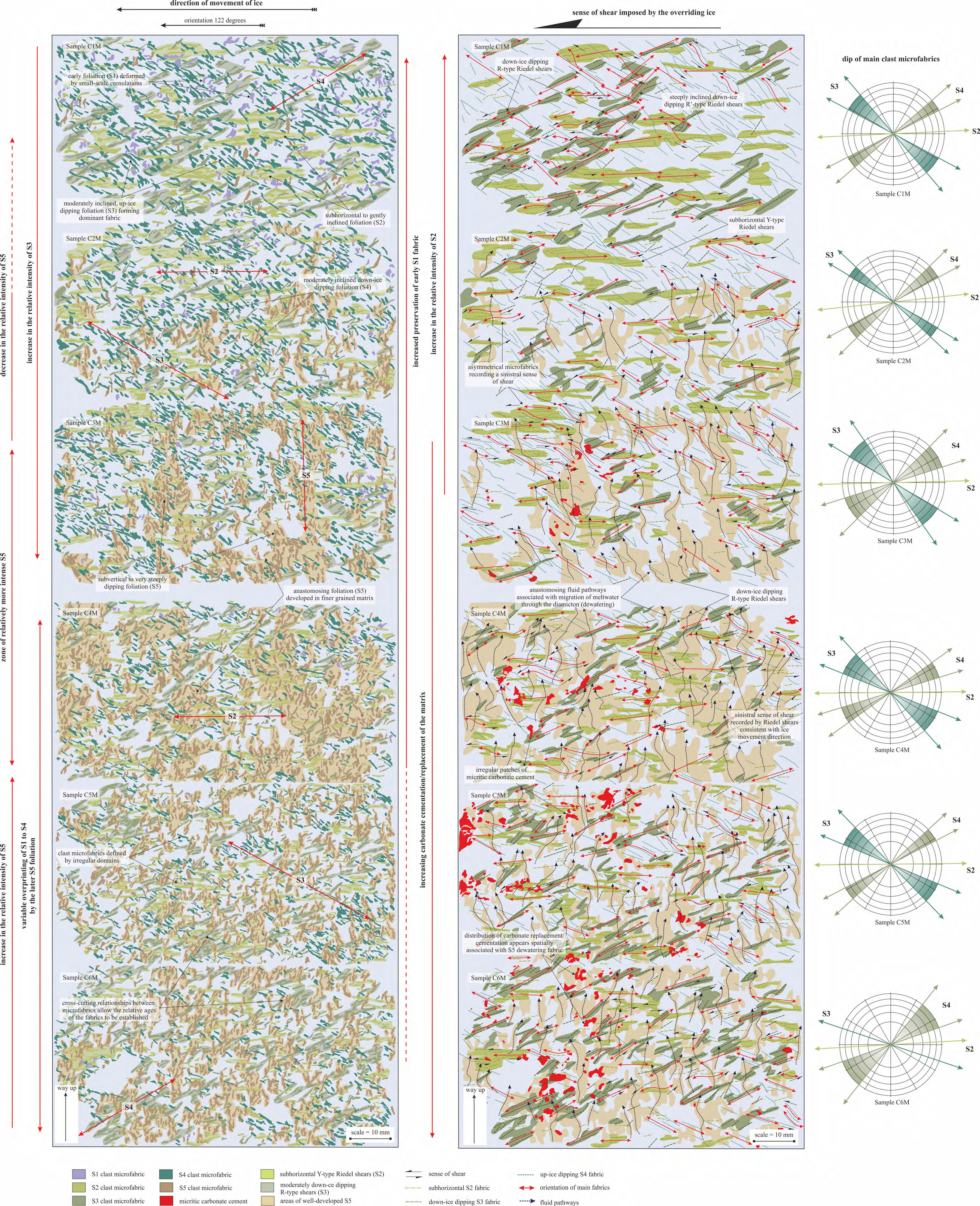

direction of movement of ice
orientation 122 degrees
sense of shear imposed by the overriding ice
Sample C1M
early foliation (S1) deformed by small-scale crenulations
S4
moderately inclined, up-ice dipping foliation (S3) forming dominant fabric
subhorizontal to gently inclined foliation (S2)
Sample C2M
S2
moderately inclined down-ice dipping foliation (S4)
S3
Sample C3M
S5
subvertical to very steeply dipping foliation (S5)
anastomosing foliation (S5) developed in finer grained matrix
Sample C4M
S2
Sample C5M
clast microfabrics defined by irregular domains
S3
Sample C6M
cross-cutting relationships between microfabrics allow the relative ages of the fabrics to be established
S4
way up
scale = 10 mm
decrease in the relative intensity of S5
increase in the relative intensity of S3
zone of relatively more intense S5
increase in the relative intensity of S5
variable overprinting of S1 to S4 by the later S5 foliation
increased preservation of early S1 fabric
increase in the relative intensity of S2
increasing carbonate cementation/replacement of the matrix
down-ice dipping R-type Riedel shears
steeply inclined down-ice dipping R'-type Riedel shears
subhorizontal Y-type Riedel shears
asymmetrical microfabrics recording a sinistral sense of shear
anastomosing fluid pathways associated with migration of meltwater through the diamicton (dewatering)
down-ice dipping R-type Riedel shears
sinistral sense of shear recorded by Riedel shears consistent with ice movement direction
irregular patches of micritic carbonate cement
distribution of carbonate replacement/cementation appears spatially associated with S5 dewatering fabric
dip of main clast microfabrics
S3
S4
S2
Sample C1M
Sample C2M
Sample C3M
Sample C4M
Sample C5M
Sample C6M
S1 clast microfabric
S2 clast microfabric
S3 clast microfabric
S4 clast microfabric
S5 clast microfabric
micritic carbonate cement
subhorizontal Y-type Riedel shears (S2)
moderately down-ce dipping R-type shears (S3)
areas of well-developed S5
sense of shear
subhorizontal S2 fabric
down-ice dipping S3 fabric
up-ice dipping S4 fabric
orientation of main fabrics
fluid pathways

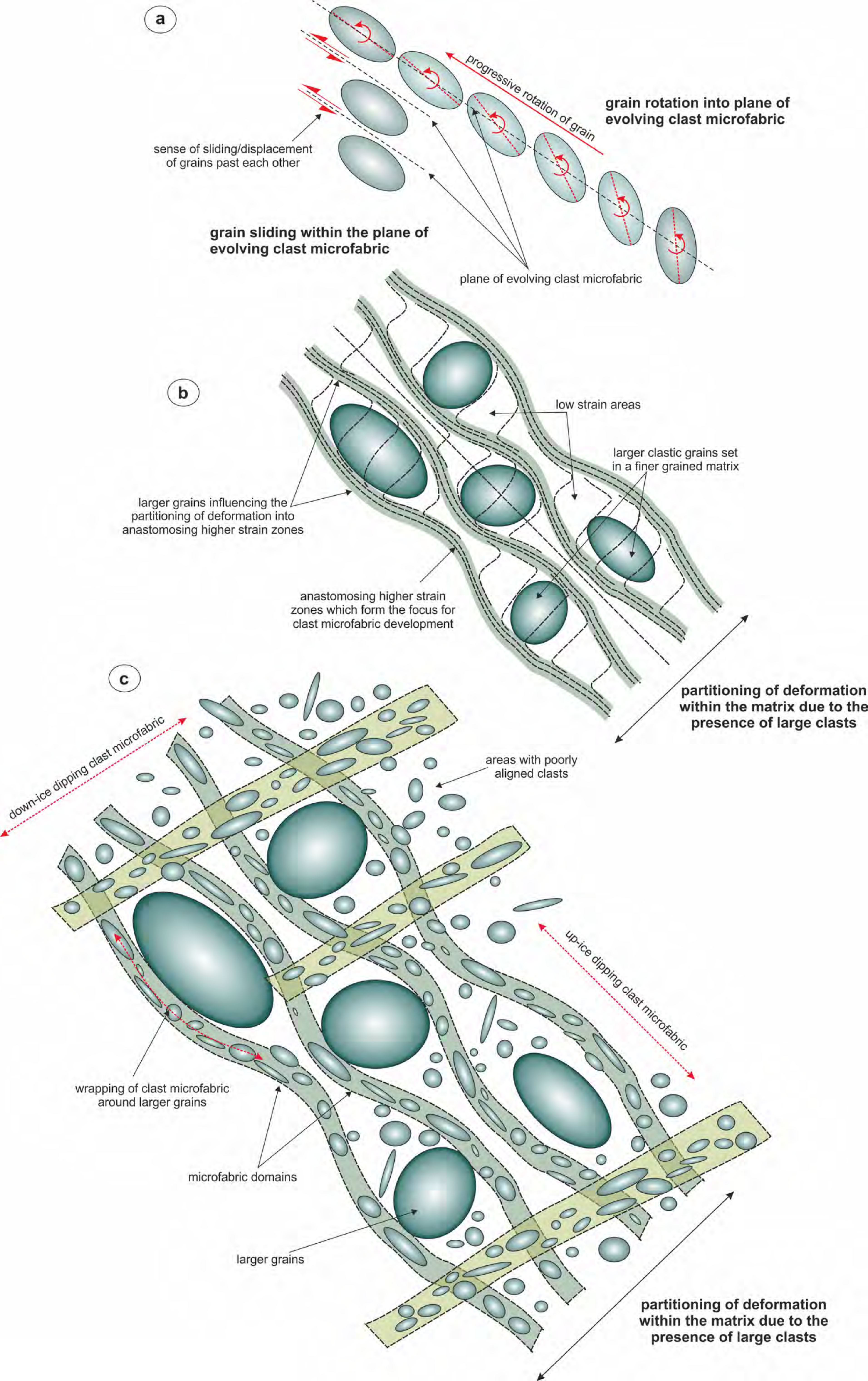
a
progressive rotation of grain
grain rotation into plane of evolving clast microfabric
sense of sliding/displacement of grains past each other
grain sliding within the plane of evolving clast microfabric
plane of evolving clast microfabric
b
low strain areas
larger clastic grains set in a finer grained matrix
larger grains influencing the partitioning of deformation into anastomosing higher strain zones
anastomosing higher strain zones which form the focus for clast microfabric development
partitioning of deformation within the matrix due to the presence of large clasts
c
down-ice dipping clast microfabric
areas with poorly aligned clasts
up-ice dipping clast microfabric
wrapping of clast microfabric around larger grains
microfabric domains
larger grains
partitioning of deformation within the matrix due to the presence of large clasts

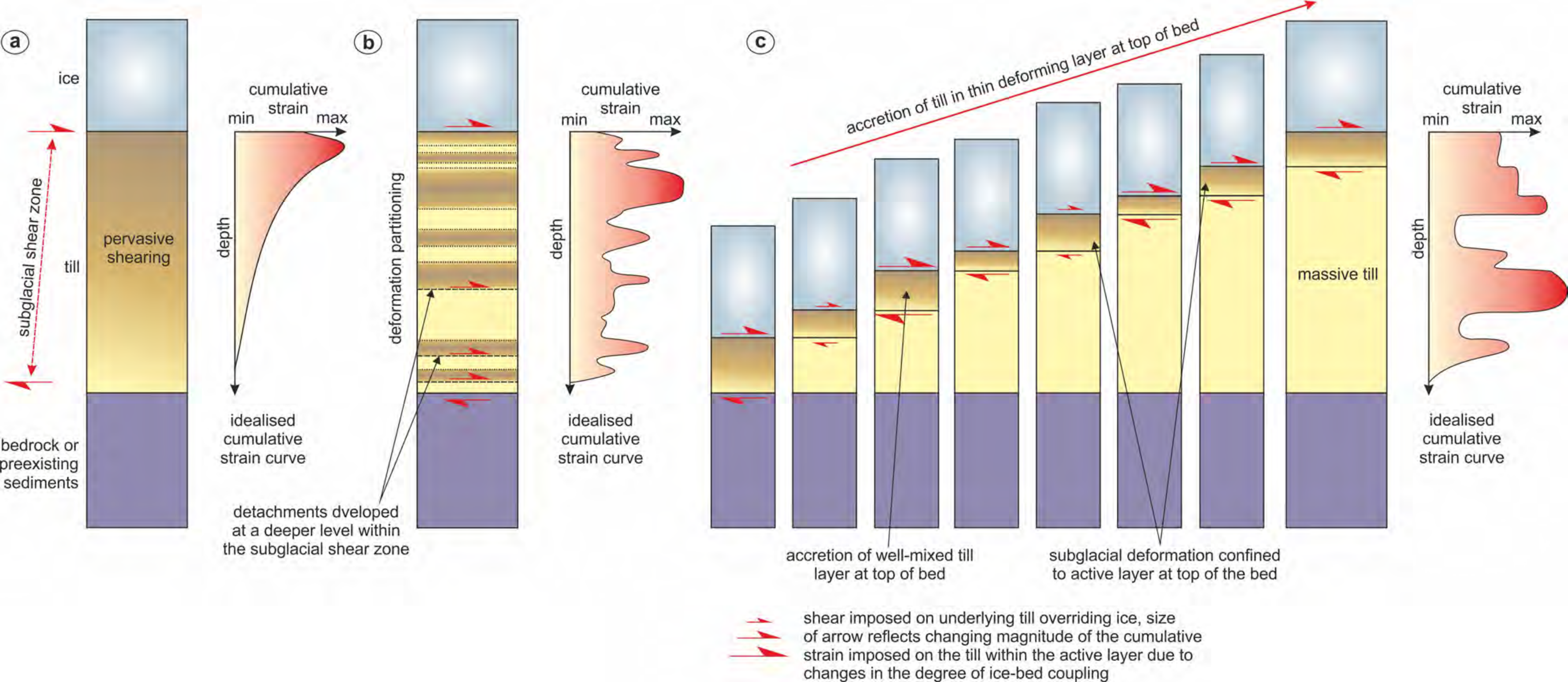

a
ice
subglacial shear zone
pervasive shearing
till
bedrock or preexisting sediments
cumulative strain
min
max
depth
idealised cumulative strain curve
b
deformation partitioning
cumulative strain
min
max
depth
idealised cumulative strain curve
detachments dveloped at a deeper level within the subglacial shear zone
c
accretion of till in thin deforming layer at top of bed
massive till
cumulative strain
min
max
depth
idealised cumulative strain curve
accretion of well-mixed till layer at top of bed
subglacial deformation confined to active layer at top of the bed
shear imposed on underlying till overriding ice, size of arrow reflects changing magnitude of the cumulative strain imposed on the till within the active layer due to changes in the degree of ice-bed coupling